NEUROSCIENCE
RESEARCH ARTICLE
W.-K. Liang et al. / Neuroscience 460 (2021) 69–87

Frontoparietal Beta Amplitude Modulation and its Interareal Cross-frequency Coupling in Visual Working Memory

Wei-Kuang Liang, [a,b,c*] **Philip Tseng,** [d,e] **Jia-Rong Yeh,** [c,f] **Norden E. Huang** [b,c,f] **and Chi-Hung Juan** [a,b,c,g]

[a] *Institute of Cognitive Neuroscience, National Central University, Taoyuan, Taiwan*

[b] *Cognitive Intelligence and Precision Healthcare Center, National Central University, Taoyuan, Taiwan*

[c] *Brain Research Center, College of Health Sciences and Technology, National Central University, Taoyuan, Taiwan*

[d] *Graduate Institute of Mind, Brain and Consciousness, Taipei Medical University, Taipei, Taiwan*

[e] *Brain and Consciousness Research Center, TMU-Shuang Ho Hospital, New Taipei City, Taiwan*

[f] *Data Analysis and Application Laboratory, The First Institute of Oceanography, Qingdao, China*

[g] *Department of Psychology, Kaohsiung Medical University, Kaohsiung, Taiwan*

Abstract—Visual working memory (VWM) relies on sustained neural activities that code information via various oscillatory frequencies. Previous studies, however, have emphasized time–frequency power changes, while overlooking the possibility that rhythmic *amplitude* variations can also code frequency-specific VWM information in a completely different dimension. Here, we employed the recently-developed Holo-Hilbert spectral analysis to characterize such nonlinear amplitude modulation(s) (AM) underlying VWM in the frontoparietal systems. We found that the strength of AM in mid-frontal beta and gamma oscillations during late VWM maintenance and VWM retrieval correlated with people's VWM performance. When behavioral performance was altered with transcranial electric stimulation, AM power changes during late VWM maintenance in beta, but not gamma, tracked participants' VWM variations. This beta AM likely codes information by varying its amplitude in theta period for long-range propagation, as our connectivity analysis revealed that interareal theta-beta couplings—bidirectional between mid-frontal and right-parietal during VWM maintenance and unidirectional from right-parietal to left-middle-occipital during late VWM maintenance and retrieval—underpins VWM performance and individual differences.

Key words: Holo-Hilbert spectral analysis, frontoparietal network, amplitude modulation, visual working memory, tDCS.

INTRODUCTION

Visual working memory (VWM) is an important cognitive faculty that sustains visual information in the mind, and enables its interaction with stored representations from long-term memory. Its integrity relies on an orchestrated effort in the maintenance and transfer of information, through local and long-distance synchronized neural activities (e.g., Aru et al., 2015; Cavanagh and Frank, 2014; Daume et al., 2017; Friese et al., 2013; Gelastopoulos et al., 2019; Hanslmayr and Staudigl, 2014; Helfrich and Knight, 2016; Onton et al., 2005; Sauseng et al., 2019). Among various oscillatory mechanisms, phase-amplitude cross-frequency coupling (CFC; aka PAC), where the *amplitude* of high-frequency brain oscillations (e.g., beta/gamma amplitude) couples with the *phase* of a low-frequency modulating wave (e.g. theta phase), has also been proposed to be one of the neural underpinnings of VWM (e.g., Axmacher et al., 2010; Fell and Axmacher, 2011; Lopes-dos-Santos et al., 2018; Roux and Uhlhaas, 2014; Siebenhühner et al., 2016; Siegel et al., 2009). However, conventional estimates of PAC (Canolty and Knight, 2010; Tort et al., 2010), though shedding light on the importance of PAC in neuroscience, have not been sufficient for representing both the low-frequency phase "modulator" and the high-frequency rhythmic amplitude "modulatee" (or the link between them both) for several reasons. First, these PAC estimates do not directly measure the rhythmic time scales of ampli-

*Correspondence to: W.-K. Liang, Institute of Cognitive Neuroscience, National Central University, Taoyuan, Taiwan.
E-mail address: wkliang@cc.ncu.edu.tw (W.-K. Liang).

Abbreviations: AM, amplitude modulation; AMF, amplitude modulation frequency/AM frequency; CBnPP, cluster-based non-parametric permutation; CF, carrier frequency; CFC, cross-frequency coupling; DQ, direct quadrature; EMD, empirical mode decomposition; HHCFPC, Holo-Hilbert cross-frequency phase clustering; HHSA, Holo-Hilbert spectral analysis; HHS, Holo-Hilbert spectrum; HHT, Hilbert-Huang transform; ICA, independent component analysis; IC, independent component; IF, instantaneous frequency; IMF, intrinsic mode function; ISPC, intersite phase clustering; lm-occipital, left middle occipital; mid-frontal, midline frontal; PAC, phase-amplitude coupling; r-parietal, right parietal; rPPC, right posterior parietal cortex; tDCS, transcranial direct current stimulation; VWM, visual working memory.

https://doi.org/10.1016/j.neuroscience.2021.02.013
0306-4522/

tude variations in high-frequency oscillation. Rather, they indirectly estimate the amplitude/power weighted statistical distribution of the high-frequency oscillation relative to the ‘‘phase” of a specified low-frequency modulating wave, which can become problematic when the amplitudes of a high-frequency oscillation are modulated by more than one low-frequency modulating wave (e.g., a gamma oscillation modulated by both theta and alpha waves at the same time). This is because the modulations resulted from different modulating waves in different time scales may interfere one another when amplitudes are represented as a distribution relative to the phase of a modulating wave in a specific time scale. Second, the phase of the low-frequency modulator is often obtained by applying Hilbert transform (or any other phase measure) on a narrowband wave that is acquired by a Fourier-based band-pass filter. The limitation here is that any conventional Fourier-based band-pass filter achieved by convolutional integrals suffers from poor temporal resolution (typically, more than two cycles), and this cannot be remedied simply by applying Hilbert transform afterward. Consequently, the ‘‘instantaneous” phase obtained by Hilbert transform remains poor in its temporal resolution.

In this study, we employed the recently-developed Holo-Hilbert spectral analysis (HHSA) (Huang et al., 2016; Nguyen et al., 2019) to directly quantify the rhythmic amplitude variations in brain oscillations during VWM as *amplitude modulations* (AMs). The HHSA is an extension of previously proposed Hilbert-Huang Transform (HHT) (e.g., Chuang et al., 2019; Huang et al., 1998, 2009; Jaiswal et al., 2019) achieved by empirical mode decomposition (EMD) and instantaneous frequency estimate with high temporal and frequency resolution, but consists of a multi-layer (here, two-layer) EMD to give a finite set of multi-layer intrinsic mode functions (IMFs) that quantifies AMs in various time scales (see Experimental procedures), generating a 3D spectral representation spanned by time, carrier frequency (CF), and AM frequency (AMF), i.e., the time-CF-AMF Holo-Hilbert spectrum (HHS). Furthermore, we employed an HHSA-based cross-frequency connectivity analysis to understand the interareal CFC in VWM. The CFC connectivity analysis is a measure similar to conventional PAC estimates, but achieved with instantaneous phases and AMs that are obtained by the two-layer EMD in HHSA. This potentially overcomes the aforementioned difficulties in representing PAC with conventional estimates.

In the current study, HHSA was applied to EEG signals acquired while participants were performing a VWM task, both before and after receiving transcranial direct current stimulation (tDCS) (Nitsche and Paulus, 2001; Tseng et al., 2012). Previously tDCS has been shown to be able to elevate low-performing participants' VWM performance, thus the current study aimed to see how well AMs can segregate participants of low and high VWM capacity (Vogel and Machizawa, 2004; Todd and Marois, 2005; Vogel et al., 2005; Sauseng et al., 2009). This EEG-tDCS data set was originally collected for investigating the effects of tDCS on event-related potentials and pre-trial alpha power in VWM (Tseng et al., 2012; Hsu et al., 2014). In light of the newly developed HHSA and HHSA-based cross-frequency connectivity analysis methods, we expect that the decoding of AM and long-range cross-frequency connectivity will not only (1) reveal the neural correlates of individual differences in VWM capacity, but also (2) shed light on the individual variabilities in people's responsiveness to the VWM enhancement effect of tDCS.

EXPERIMENTAL PROCEDURES

Twenty participants performed a standard change detection task (Fig. 1A) with their EEG signals recorded. The experiment consisted of two sessions, performed on two separate days: one with anodal tDCS over right posterior parietal cortex (rPPC; Fig. 1B, first graph), and the other without real tDCS (sham condition). Participants' VWM capacity was evaluated by Pashler's *K*, which estimated the number of remembered items [for details please see the *Behavioral measures* in supplementary information (SI) Appendix] (Pashler, 1988; Luck and Vogel, 1997; Rouder et al., 2011).

EEG data recorded along the two sessions were first analyzed by independent component analysis (ICA) (Makeig et al., 1996; Hyvarinen and Oja, 2000; Delorme and Makeig, 2004), followed by organizing independent components (ICs) obtained from all participants into clusters based on their similarities (Hyvarinen, 2011; Hyvarinen and Ramkumar, 2013). Three clusters that represented midline frontal (mid-frontal), left middle occipital (lm-occipital), and right parietal (r-parietal) brain activities (Fig. 1C; please see the following *Independent component analysis* for details) were chosen for the following HHSA (in the IC clustering, only the three chosen clusters and one cluster that represented vertical ocular activity were complete, i.e., each cluster involved ICs from all participants). After performing HHSA on the chosen ICs, to adequately visualize and perform statistical analysis on the result of HHSA, we produced the marginal HHS by summing/averaging the 3D time-CF-AMF spectrum over either a specific or the entire range of a given dimension (i.e., CF/AMF). All statistical analyses employed here were based on a standard cluster-level non-parametric statistic (Maris and Oostenveld, 2007; Groppe et al., 2011) under the criterion of cluster $\alpha < 0.05$, two-sided. Unless specifically mentioned, only ‘‘hit” trials were analyzed. Colorbars for statistical results (e.g., *T* value, and correlation coefficient *r*) of HHS are shown with ticks of values corresponding to $p < 0.05$, 0.01, and 0.001, two-tailed, uncorrected level on both positive and negative direction.

Participants

The required sample size was estimated (Hulley et al., 2007) to be 19 for a predictive statistical power of 0.81 when the expected correlation coefficient between behavioral and neurophysiological data is 0.60 under the criteria $\alpha = 0.05$ (two-tailed) and $\beta = 0.20$ (α: the probability of committing a type I error, and β: the probability of making a type II error). Thus, twenty college students with normal/

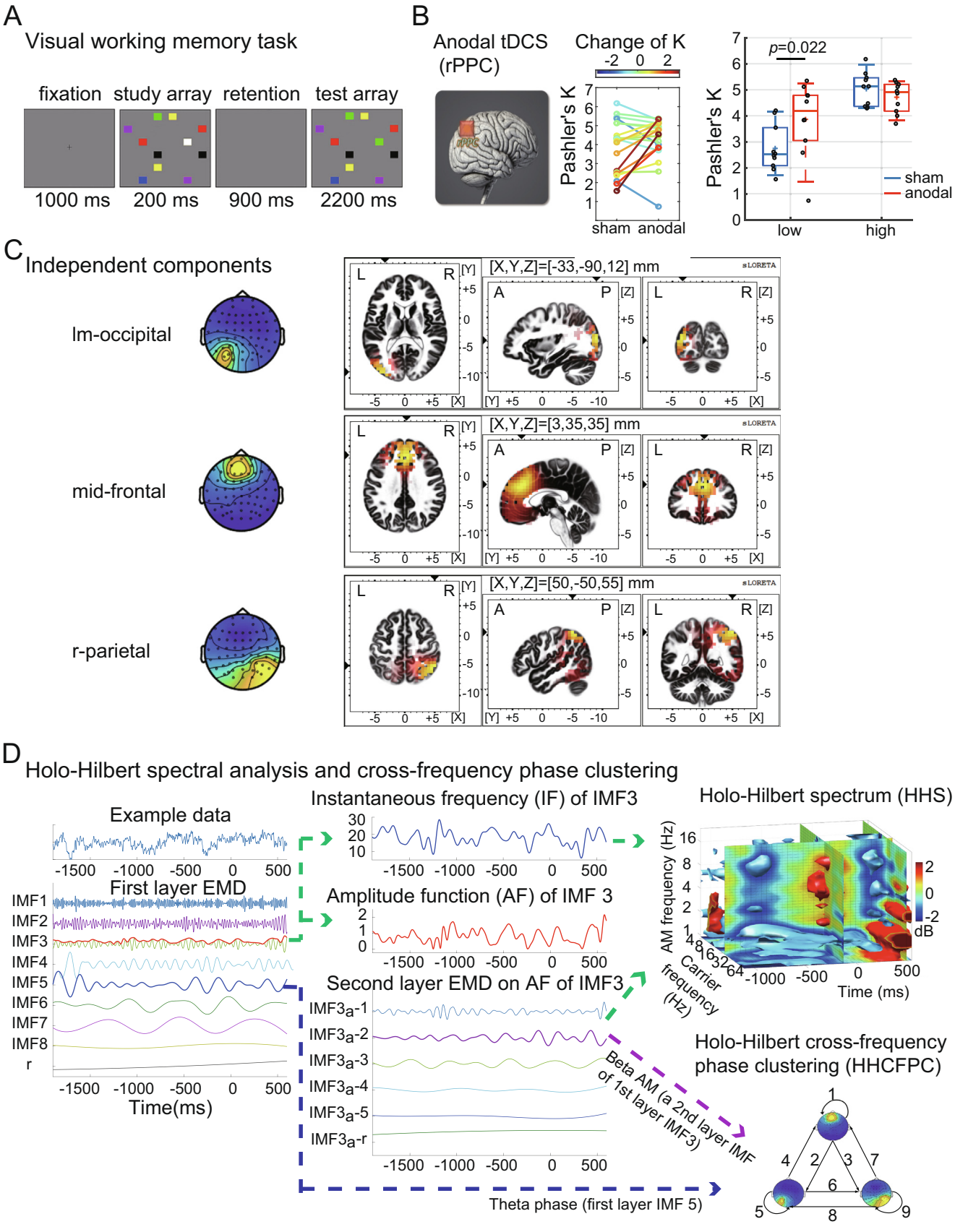
A
Visual working memory task
fixation
study array
retention
test array
1000 ms
200 ms
900 ms
2200 ms
B
Anodal tDCS
(rPPC)
rPPC
Change of K
-2 0 2
Pashler's K
sham anodal
p=0.022
low
high
sham
anodal
C
Independent components
lm-occipital
mid-frontal
r-parietal
[X,Y,Z]=[-33,-90,12] mm
[X,Y,Z]=[3,35,35] mm
[X,Y,Z]=[50,-50,55] mm
sLORETA
D
Holo-Hilbert spectral analysis and cross-frequency phase clustering
Example data
First layer EMD
IMF1
IMF2
IMF3
IMF4
IMF5
IMF6
IMF7
IMF8
r
Time(ms)
Instantaneous frequency (IF) of IMF3
Amplitude function (AF) of IMF 3
Second layer EMD on AF of IMF3
IMF3a-1
IMF3a-2
IMF3a-3
IMF3a-4
IMF3a-5
IMF3a-r
Holo-Hilbert spectrum (HHS)
AM frequency (Hz)
Carrier frequency (Hz)
Time (ms)
dB
Beta AM (a 2nd layer IMF of 1st layer IMF3)
Theta phase (first layer IMF 5)
Holo-Hilbert cross-frequency phase clustering (HHCFPC)

corrected-to-normal vision were recruited to participate in the experiment (mean age = 22; all were neurologically normal; 13 females). Informed consent was acquired from every participant before the experiment. The experiment and tDCS procedure were approved by the Institutional Review Board of the Chang-Gung Memorial Hospital (Taoyuan, Taiwan).

VWM task, tDCS, and data acquisition

Participants' VWM performance was measured with a standard change detection task consisted of 144 trials during each of the sham and anodal tDCS session. In each trial, participants first saw a fixation cross (1000 ms), followed by the memory array (200 ms), retention interval (900 ms), test array (2200 ms), and inter-trial interval (1000 ms) (Fig. 1A). Participants were required to remember 11 rectangular colored items presented in the memory array, and judge whether any one of the items had changed color in the test array. The entire memory/test array extended approximately 31°×24°, with each item sized at 1.6°×1.3° visual angle. Color of each item was randomly selected from a pool of 7 highly-distinguishable colors (black, blue, green, red, violet, white, and yellow), and each color was programmed to occupy only one or (at most) two items in each array and trial.

In this experiment, tDCS was delivered by a Neuroconn Eldith DC-stimulator with saline-soaked sponges (4 × 4 cm). The anodal and sham tDCS sessions were carried out at least 24 h apart, with counterbalanced order across all participants. The center of the anodal tDCS electrode was placed over P4 (localized with the international 10–20 system of EEG), with the reference electrode positioned on the left cheek (Tseng et al., 2012). A current of 1.5 mA was applied for 15 min, in addition to a 15 s fade-in and 15 s fade-out time, resulting in 15.5 min of anodal tDCS. The duration of the sham tDCS was the same as the active session, but with only the fade-in and fade-out durations (30 s total). Both the stimulation strength and the current density were below the safety criterion (Nitsche and Paulus, 2001; Nitsche et al., 2008; Bikson et al., 2016; Antal et al., 2017).

After the application of anodal/sham tDCS, participants rested for 30–120 s as the experimenters removed the tDCS electrodes and readjusted nearby EEG electrodes. Participants then started on the VWM task, with concurrent recording of their EEG data. EEG signals were recorded with Ag/AgCl electrodes mounted on a 64-channel elastic cap (Electrocap International) according to the international 10–20 system. All channels were referenced to an electrode positioned between Cz and CPz. The impedance of each EEG electrode was kept below 5 kΩ. A Neuroscan amplifier and its built-in Neuroscan 4.2 software were used for data acquisition with a sampling rate of 1000 Hz and bandpass filtering from 0.05 to 70 Hz. Ocular artifact rejection was performed to exclude trials with eye blinks (VEOG amplitude $> \pm 50\ \mu V$) or horizontal eye movement (HEOG amplitude $> \pm 50\ \mu V$, or peak-to-peak amplitude > 16 μV). After that, the acquired data were re-referenced offline to the average of M1 and M2.

Data preprocessing

The continuous EEG data were epoched from 800 ms prior to, and 1700 ms after, the onset of the study array. EEG data of each epoch were further detrended by EMD (i.e. removing the trend of the data, the effect was similar to applying a 0.3 Hz high-pass filter to the data, but without distorting any oscillatory characteristics of the outputs). After the detrending process, trials containing artifacts exceeding $\pm 150\ \mu V$ were rejected. Finally, EEG data of each channel were further re-referenced to the average of all EEG channels (i.e., the averaged reference).

Independent component analysis

The aim of the present study is to reveal the importance of AMs in brain oscillations during VWM. Although AMs should originate from a process of multiplication, however, it could also be a result of summation over many oscillations with different but close frequencies. To keep the source of brain oscillations as pure as possible, ICA (Makeig et al., 1996; Hyvarinen and Oja, 2000) was applied to single-subject EEG data. The independent components (ICs) obtained by the ICA have

Fig. 1. Illustration of the visual working memory task, tDCS, behavioral result, ICA components, and the procedure of HHSA and HHCFPC. **(A)** The task began with a fixation cross, followed by the memory array, retention interval, test array, and inter-trial interval. **(B)** Two experimental sessions were performed on two separate days: one with anodal tDCS over rPPC (first graph) and the other without real tDCS to serve as the sham tDCS condition. From the perspective of the entire sample of participants, anodal tDCS did not significantly improve participants' VWM capacity ($p = 0.158$, paired t-test, two-tailed) (second graph). When participants were divided into a high-performing and low-performing group, anodal tDCS showed a facilitative effect for low performers ($p = 0.022$, paired t-test, two-tailed; Hedges's $g = 0.86$), but not for high performers ($p = 0.105$; Hedges's $g = 0.47$) (third graph; shown by box-and-whisker plots of Pashler's K values, with the box depicting the median and the 25th and 75th quartiles and the whisker showing the 5th and 95th percentile) **(C)** EEG data were first analyzed by ICA, followed by organizing ICs obtained from all participants into IC clusters based on their similarities. Three complete IC clusters (i.e., each cluster involved ICs from all participants) that represented midline frontal (mid-frontal), left middle occipital (lm-occipital), and right parietal (r-parietal) brain activities were chosen for the following HHSA. The brain source of the topography of each chosen cluster was estimated by sLORETA. **(D)** The HHSA consists of a procedure of two-layer EMD to give a finite set of two-layer IMFs that quantifies AMs in various time scales, generating a full dimensional spectral power representation in a 3D space spanned by time, carrier frequency (CF), and AM frequency (AMF). Furthermore, by using an HHSA-based CFC analysis (i.e. HHCFPC), we were able to examine the cross-frequency connectivity in the frontoparietal system.

been proposed to have characteristics of statistical-independent time series and near-dipolar scalp topographies (Makeig et al., 2004; Delorme et al., 2012). As a result, ICA transforms the multi-channel EEG data into time series of brain areal activities, as well as that of non-brain activities, potentially avoiding effects derived from mixed sources. Therefore, after ICA, any further analysis can be applied to time courses of ICs that are more likely to be activities within individual cortical areas (Delorme et al., 2012).

In the present study, the logistic infomax ICA (Bell and Sejnowski, 1995) built in EEGLAB (i.e. the *runica* program) was applied to EEG data concatenated from all change trials between 800 ms prior to the memory array onset and 600 ms after the start of test array (i.e. a length of 2500 ms in a trial). The ICA was preceded by a principal component analysis (PCA) which reduced the dimensionality of the EEG data to 48. For every subject, the EEG data reconstructed by the 48 principal components retained at least 99% of the total variance while suppressing unrelated noises from the original EEG data. This resulted in 48 ICs in the subsequent ICA for each subject. To further perform group analysis on the results of single-subject ICA, a method that tests the inter-subject consistency of ICs (ISCTEST) (Hyvarinen, 2011; Hyvarinen and Ramkumar, 2013) was employed to find clusters of ICs that were sufficient similar in their mixing coefficients across subjects. The null hypothesis of the test was that the ICs are random orthogonal components in the whitened space. We employed the method by the code acquired from https://www.cs.helsinki.fi/u/ahyvarin/code/isctest/, and kept its default parameters that used a single-linkage strategy by which the sufficiency of similarity was tested by controlling both the corrected false positive rate (FPR) and the false discovery rate (FDR) at the level of 0.05 (Hyvarinen, 2011).

For the current dataset, 18 clusters of ICs were identified by the ISCTEST (SI Fig. S1). Among them clusters 1–4 are "complete", i.e., every participant has exactly one corresponding IC in each of the clusters. To include all participants in the following analysis, only ICs in the complete clusters 2–4 were recruited. ICs in cluster 1 were related to vertical eye movements (SI Table S2) and were thus not included in subsequent analysis. The brain sources of the topography of each chosen cluster (Fig. 1C, first graph) was estimated by sLORETA (Pascual-Marqui, 2002), demonstrating that the sources were best localized to left middle occipital gyrus (lm-occipital; maximum standardized power in MNI coordinate system: [−33, −90, 12] mm), medial frontal gyrus (mid-frontal; [3, 35, 35] mm), and right parietal lobe (r-parietal; [50, −50, 55] mm) (Fig. 1C) for the three chosen clusters, respectively.

HHSA method

In the present study, HHSA was employed to represent AMs in the EEG data. Instead of carrying out HHSA on brain signals from EEG channels, here the HHSA was applied to the time course of each IC within each epoch, and only to those ICs in the complete IC clusters. In the following, the time courses of ICs will be regarded as signals at "virtual electrodes".

The HHSA includes a process of multiple-layer nested EMD (Huang et al., 2016) and a high-dimensional spectral representation. In this study, EMD of two nested layers was performed. The steps of the two layer EMD are summarized as follows:

a. The first layer EMD is applied to signals of each IC by an enhanced algorithm of EMD [eEMD (Deering and Kaiser, 2005; Tsai et al., 2016); for details, please see the SI text], which decomposes the signals from each IC into a collection of IMFs (see Fig. 1D, left). The first layer EMD can be given as

$$x(t) = \sum_{j=1}^{n} c_j(t) + r_n = \sum_{j=1}^{n} a_j(t)\cos\theta_j(t) + r_n,$$

in which the original signal $x(t)$ is decomposed into n IMFs, and the jth IMF, $c_j(t)$, can be expressed as $a_j(t)\cos\theta_j(t)$, where $a_j(t)$ is the amplitude function obtained by a cubic spline algorithm, $\theta_j(t)$ is the phase function determined by direct quadrature (DQ) (Huang et al., 2009), and r_n is the trend without any oscillatory characteristics. The instantaneous frequency (IF) of the jth IMF is defined as the time derivative of the phase function, $\theta_j(t)$. This step is similar to previous implementations of HHT (Huang et al., 1998).

b. The second layer EMD in HHSA is implemented by applying eEMD to the amplitude function of each IMF obtained from the first layer EMD (Fig. 1D, middle), given as

$$a_j(t) = \sum_{k=1}^{l_2} a_{jk}(t)\cos\Theta_{jk}(t) + R_{jl_2},$$

where the *j*th first layer IMF's amplitude function, $a_j(t)$, is decomposed into l_2 second layer IMFs, and each second layer IMF can be expressed as $a_{jk}(t)\cos\Theta_{jk}(t)$, where $a_{jk}(t)$ is the second layer amplitude function, $\Theta_{jk}(t)$ is the second layer phase function, and R_{jl_2} is the second layer trend corresponding to the second layer IMF. The corresponding instantaneous "AM frequency" is defined as the time derivative of the second layer phase function, $\Theta_{jk}(t)$. This step is referred to as "AM expansion", expanding each first layer amplitude function into *amplitude modulations* in various time scales. Taken together, the two-layer EMD can be expressed as a nested form:

$$x(t) = \sum_{j=1}^{n}\left[\sum_{k=1}^{l_2} a_{jk}(t)\cos\Theta_{jk}(t) + R_{jl_2}\right]\cos\theta_j(t) + r_n,$$

We note that only when a first layer IMF is free from the problem of mode mixing, can its amplitude function be reliably constructed for the subsequent second layer EMD (Huang et al., 2016). Moreover, to emphasize the concept of instantaneous "AM frequency" in the second layer EMD and to avoid confusion, we will refer to the instantaneous frequency obtained from the first layer EMD as "carrier frequency" when it is represented as a dimension in HHS.

Although all the oscillatory information such as IMFs, first and second layer amplitude function, instantaneous

frequency, and instantaneous AM frequency (along with instantaneous phase and instantaneous AM phase, if required) in both first and second layer EMD have been acquired in the two steps above, there remains the need for a spectral representation to integrate all the given information. The spectral representation in HHSA is as follows:

c. All the oscillatory information obtained from the two-layer EMD are represented as an AM power distribution in a 3D space spanned by time, carrier frequency (CF), and AM frequency (AMF) according to the instantaneous AM frequency and second layer amplitude function obtained from the second layer EMD, as well as the instantaneous frequency acquired from the first layer EMD. It should be noted that the dimension of "carrier frequency" here would correspond to the *frequency* dimension in conventional time–frequency spectral analyses. The three dimensional power distribution is referred to as the 3D Holo-Hilbert spectrum (HHS).
d. To better visualize and organize the data for further statistical analysis, the marginal sum/mean of the 3D HHS could be taken as 1) over the dimension of AMF (or a specific range of AMF); 2) over the dimension of time (or a specific window of time); or 3) over the dimension of CF (or a specific range of CF), generating the marginal HHS on the 2D time-CF, CF-AMF, or time-AMF subspace, respectively.

Because the temporal information is critical for understanding the oscillatory dynamics in VWM, the current study primarily used the time-CF and time-AMF marginal HHS to demonstrate the EEG data during VWM. The time-CF HHS was produced by taking the marginal sum over the entire AM frequency range, because of the completeness and orthogonality of IMFs, the result was consistent with the previously proposed HHT time–frequency spectral power (Huang et al., 2016). Regarding the time-AMF HHS, since VWM related rhythmic amplitude variations were primarily found in high-frequency brain oscillations (e.g., Friese et al., 2013; Lopes-dos-Santos et al., 2018), in this study the marginal sum was taken over either the beta (13.5–24 Hz) or gamma (25–50 Hz) range of CF. Consequently, because of the fact that AMF should be smaller than CF (i.e., $\frac{d\Theta_{jk}}{dt} < \frac{d\theta_j}{dt}$) the AMF range that characterized the rhythmic amplitude variations (i.e., AMs) were set from 0-12.3 Hz and from 0-24.7 Hz for beta and gamma oscillations, respectively. Because a number of prior studies have demonstrated the roles of theta and alpha oscillations in VWM by conventional time–frequency analyses (e.g., Cavanagh and Frank, 2014; Hsu et al., 2014; van Ede et al., 2017), we expect that the time-CF HHS to be sufficient to represent low-frequency brain oscillations (i.e., delta, theta, and alpha bands) in VWM. We also expect that the time-AMF HHS to be more proficient in revealing VWM-related high-frequency brain oscillations (i.e., beta, and gamma bands) that consist of pronounced AM effects. In the present study both the carrier and AM frequency bins are log2-scaled. The lowest AM frequency bin, denoted as "trend_{AM}", was placed at the bottom of the HHS and separated from other bins. This is because trend_{AM} represents the "unmodulated" power computed by the trend (i.e., the last component) of each second-layer EMD, where instantaneous AM frequency is not defined (or, 0 Hz).

The marginal time-CF, and time-AMF HHS were first averaged over trials in each condition. To improve the normality of the spectral power for further statistical analysis, the averaged marginal time-CF or time-AMF HHS were then rescaled to the logarithm of the ratio of spectral power to the averaged power over the time window between 600 ms prior to the memory array onset and 550 ms after the test array onset. The use of the time series from almost the entire trial instead of a pretrial period as the baseline is because that oscillatory activities in the late fixation period has been shown to be critical for VWM in previous studies [e.g., pre-trial alpha power (Hanslmayr et al., 2007; Hsu et al., 2014; van Ede et al., 2017)], hence the choice of a baseline window within the fixation period is not appropriate for the present task.

Further, since HHS separates oscillatory power into AM power (characterized by its rhythmic patterns) and unmodulated power (majority of sustained changes in power), the current study that aims to reveal AM power in VWM may need to emphasize phasic changes in activity. Therefore, we chose the time series from the entire trial as the baseline both for keeping the possible effect during the fixation period visible and for revealing phasic changes in AM power.

Holo-Hilbert cross-frequency phase clustering

To understand the VWM underpinnings from a network perspective, in this study we also employed Holo-Hilbert cross-frequency phase clustering (HHCFPC), a CFC connectivity analysis that is based on HHSA. The HHCFPC was adapted from the conventional "intersite phase clustering" (ISPC) (Lachaux et al., 1999; Cohen, 2014; Vidaurre et al., 2018) that averages phase angle differences between two series of phase data over *time*. But, instead of clustering phase differences between two sites from the same frequency band, the HHCFPC clustered the vectors of "phase difference" between the phase function of a first layer IMF from one site (in this study, an IC) and the phase function of a *scale-matched* second layer IMF (decomposed from the amplitude function of its corresponding first layer IMF) from the same or the other site. The scale matching was achieved by finding a second layer IMF at the second site with its averaged instantaneous AM frequency closest to the averaged instantaneous frequency of the first layer IMF at the first site. The equation of HHCFPC is as follows:

$$\text{HHCFPC} = \left| n^{-1} \sum_{t=1}^{n} e^{-i\left(\theta_{i:t}|_x - \Theta_{jk:t}|_y\right)} \right|$$

in which n is the number of time points, and $\theta_{i:t}|_x$ and $\Theta_{jk:t}|_y$ are phase angles from the ith first layer IMF of site x and the scale-matched second layer IMF (suppose its order is k) decomposed from amplitude function of the jth first

layer IMF of site *y*, respectively. We note that the scale-matched second layer IMF at the second site can only be meaningful if the instantaneous frequency of its corresponding first layer IMF is higher than the instantaneous frequency of the first layer IMF at the first site (i.e., $j < i$ in the equation of HHCFPC – the lower order IMF has higher instantaneous frequency), because the instantaneous AM frequency of any given second layer IMF must be lower than the instantaneous frequency of its corresponding first layer IMF. Take the current study as example, HHCFPC between the first layer IMF 5 [maximum likelihood (ML) and maximum entropy (ME) object of theta band] from the r-parietal IC and the first layer IMF 3 (ML and ME object of beta band) from the mid-frontal IC was obtained by computing the phase clustering between the phase of the first layer IMF 5 at the r-parietal IC and the phase of a "theta-scale" second layer IMF of the first layer IMF 3 at the mid-frontal IC.

In the present study, HHCFPC was systematically computed in sliding time segments of 600 ms in length, and by steps of 100 ms for each possible pair of ICs (i.e. ICs from the mid-frontal, lm-occipital, and r-parietal clusters) between the 5th first layer IMF (i.e. theta oscillation) at one IC and the 2nd/3rd first layer IMF (i.e. gamma/beta oscillation) at the other IC. The chosen segment length allowed approximately three cycles of the 5th first layer IMF (i.e. theta oscillation) according to the peak IF in its frequency distribution.

Statistical analysis

We performed a standard cluster-based non-parametric permutation (CBnPP) test (Maris and Oostenveld, 2007; Groppe et al., 2011) to reveal the differences of HHS/HHCFPC between two conditions, and to evaluate the correlations between the HHS/HHCFPC and VWM performance. Originally, this method was applied to control the family-wise error rate (FWER) in E/MEG data by clustering test results (e.g., *t* values, or correlation coefficient) across nearby sensors and time points based on a pre-specified uncorrected threshold of statistical level. The current employment of this method is as follows:

For HHSA: In any 2D marginal representation of HHS (i.e., the CF-AMF, time-AMF, or time-CF HHS), two adjacent pixels along the vertical, horizontal, or diagonal direction on the HHS were identified as neighbors, and a cluster was formed both by the relationship of neighborhood and an uncorrected threshold of $p < 0.05$ (two-tailed) in a test.

For HHCFPC: In the time-connectivity representation of HHCFPC, the test was achieved by grouping the test results at nearby "connections" and time points into clusters. In this study, neighbors of a directional connection were defined as connections that shared either the same starting node or the same ending node with the specified connection of interest. In addition, any connection's reciprocal connection was also included in its set of neighbors.

The null distribution was generated by 5000 permutations on participants' conditions in a dependent samples t-statistic or on participants' order in a correlation analysis, and for each permutation the maximum cluster-level statistic was computed. Finally, the original (i.e., without permutation) cluster-level statistic was further tested against the null distribution under the significance level $\alpha = 0.05$, two-sided.

Data availability

Custom MATLAB codes for HHSA and a minimal set of data that can be used for replicating the main findings of the present study are available from the corresponding project in the public repository: https://osf.io/mg6zd/ (DOI: 10.17605/OSF.IO/MG6ZD). In this project the subfolder "hhsa_tools_d2" contains a set of necessary functions (including an installation guide and an installing script: "install_hhsa.m") for performing HHSA together with their wrappers for analyzing data in SPM12 format (http://fil.ion.ucl.ac.uk/spm/). If these functions are correctly installed, by following the steps described on the "Home" page of the project, readers should be able to reproduce main findings in the current study. These codes and data are open access under the GNU general public license (GPL) v2.0.

RESULTS

Behavioral results

Participants varied broadly in their VWM capacity, with Pashler's *K* ranging from 1.56 to 6.18 (mean = 3.89; $SD = 1.40$) in the sham condition. From the perspective of the entire sample of participants, anodal tDCS (mean = 4.29; $SD = 1.14$) did not significantly improve participants' VWM capacity ($p = 0.158$, paired *t*-test, two-tailed; Fig. 1B, second graph). However, when participants were divided into a high-performing and low-performing group using a median split based on their natural VWM capacity (i.e., Pashler's *K* in sham condition), anodal tDCS showed a facilitative effect for low performers ($p = 0.022$, paired *t*-test, two-tailed; Hedges's $g = 0.86$), but not for high performers ($p = 0.105$; Hedges's $g = 0.47$) (Fig. 1B, third graph). In the low-performing group, 8 out of 10 individuals showed a boost of 0.59–2.99 to their Pashler's *K* from anodal tDCS, whereas only 2 in 10 individuals in the high-performing group showed an increment between 0.13 and 0.73 in Pashler's *K*. This observation demonstrates individual differences in responsiveness to anodal-tDCS (Hsu et al., 2016; Tseng et al., 2018), and is further supported by a significant interaction observed in a 2×2 mixed-design ANOVA for tDCS (anodal vs. sham) and performance (high- vs. low-performing) in *K* (*interaction*: $F_{(1,18)} = 10.70$, $p = 0.0042$, partial $\eta^2 = 0.373$; tDCS: $F_{(1,18)} = 3.26$, $p = 0.088$, partial $\eta^2 = 0.153$; and performance: $F_{(1,18)} = 18.76$, $p = 0.0004$, partial $\eta^2 = 0.51$). For a more detailed summary of behavioral results, please see the SI Table S1.

VWM performance is correlated with r-parietal theta oscillatory power

We first generated the time-CF marginal HHS by summing the AM power over the entire AMF dimension

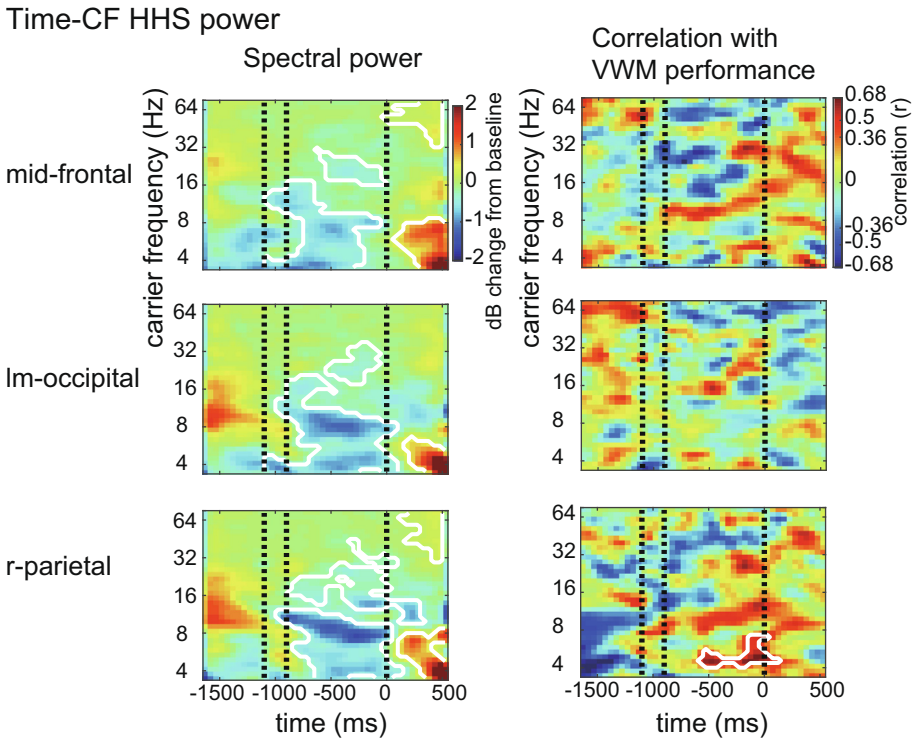

Fig. 2. Time-CF HHS for the mid-frontal, lm-occipital, and r-parietal brain oscillations during the process of VWM, and their correlations with VWM performance. The time-CF HHS showed a significant positive correlation between r-parietal theta power and the VWM performance during VWM maintenance (cluster $p = 0.04$, peak $r = 0.73$; significant cluster was surrounded by a white contour).

in the 3D HHS. This time-CF HHS is consistent with our previously proposed HHT time–frequency spectrum (Huang et al., 1998, 2016), which is incapable of representing AM effects. Fig. 2 shows the grand averaged time-CF HHS for the mid-frontal, lm-occipital, and r-parietal brain oscillations during the process of VWM, and their correlations with VWM performance. A positive correlation between r-parietal theta power during VWM maintenance and VWM performance (cluster $p = 0.04$, peak $r = 0.73$; significant cluster surrounded by white contour) is clearly revealed. As expected, the AM effects in high frequency oscillations (i.e. beta and gamma) is not clear in this representation because the dimension of AMF is collapsed. As indicated in the 2016 study by Huang et al., all existing time–frequency analyses are unable to quantitatively represent AM effects. This point is exemplified in SI Fig. S2, where we show wavelet time–frequency spectrum for the current task.

VWM performance is correlated with AMs in mid-frontal beta and gamma oscillations

To investigate the relationship between AMs in beta or gamma brain oscillation and VWM, we analyzed the 2D time-AMF marginal HHS by summing the AM power of the 3D HHS over the carrier frequencies within the beta (13.5–24 Hz), or gamma (25–50 Hz) range. The time-AMF HHS for the mid-frontal, lm-occipital, and r-parietal *beta* AMs are shown in Fig. 3A (top), demonstrating a pattern of two-phase desynchronization during the early maintenance and retrieval stages with AM frequency higher than 2 Hz, as well as a process of desynchronization in the encoding and maintenance stage first, then re-synchronizes in the retrieval stage with AM frequency lower than 2 Hz. Specifically, in the r-parietal beta AM, a synchronized pattern with AM frequency higher than 2 Hz during late VWM maintenance is observed (top, third graph). The correlation analyses indicate significant *positive* correlation between the time-AMF HHS of *mid-frontal beta* AMs and participants' VWM performance within two ranges of AM frequencies (i.e. 1.5–2 and 3–4 Hz) during VWM retrieval (Fig. 3A, middle, first graph), both of which may have originated from a range of AM frequency 1.8–4 Hz during the late maintenance stage (cluster $p = 0.01$, peak $r = 0.66$; highlighted by white contour). Further, the within-subjects contrast between the Hit and Miss conditions indicates that the AM power in AM frequency 3.5–7 Hz of beta oscillations during the early VWM maintenance is higher for the Hit than Miss condition (Fig. 3A, bottom, first graph).

The time-AMF HHS for *gamma* oscillations is shown in Fig. 3B (top). The correlation analysis between the time-AMF HHS of mid-frontal *gamma* AMs and participants' VWM performance (Fig. 3B, middle, first graph) revealed that the AM power within AM frequency 1.5–2 Hz was first negatively correlated with the VWM performance during memory encoding and early maintenance, then *positively* correlated with the VWM performance during the late maintenance and retrieval stage (cluster $p = 0.029$ and 0.01, respectively). However, the contrast between the Hit and Miss conditions for the time-AMF HHS of mid-frontal gamma AMs is not as significant statistically as beta AMs. These correlations between the time-AMF HHS and VWM performance suggest that individual differences in VWM capacity may be reflected in the mid-frontal beta/gamma AMs.

Individual differences in VWM performance are revealed by AMs in mid-frontal beta and gamma, and r-parietal beta oscillations

To further investigate whether individual differences (Unsworth and Engle, 2007, 2008) in VWM can be revealed and classified via beta/gamma AMs, we divided the participants into a low-performing ($N = 10$; mean

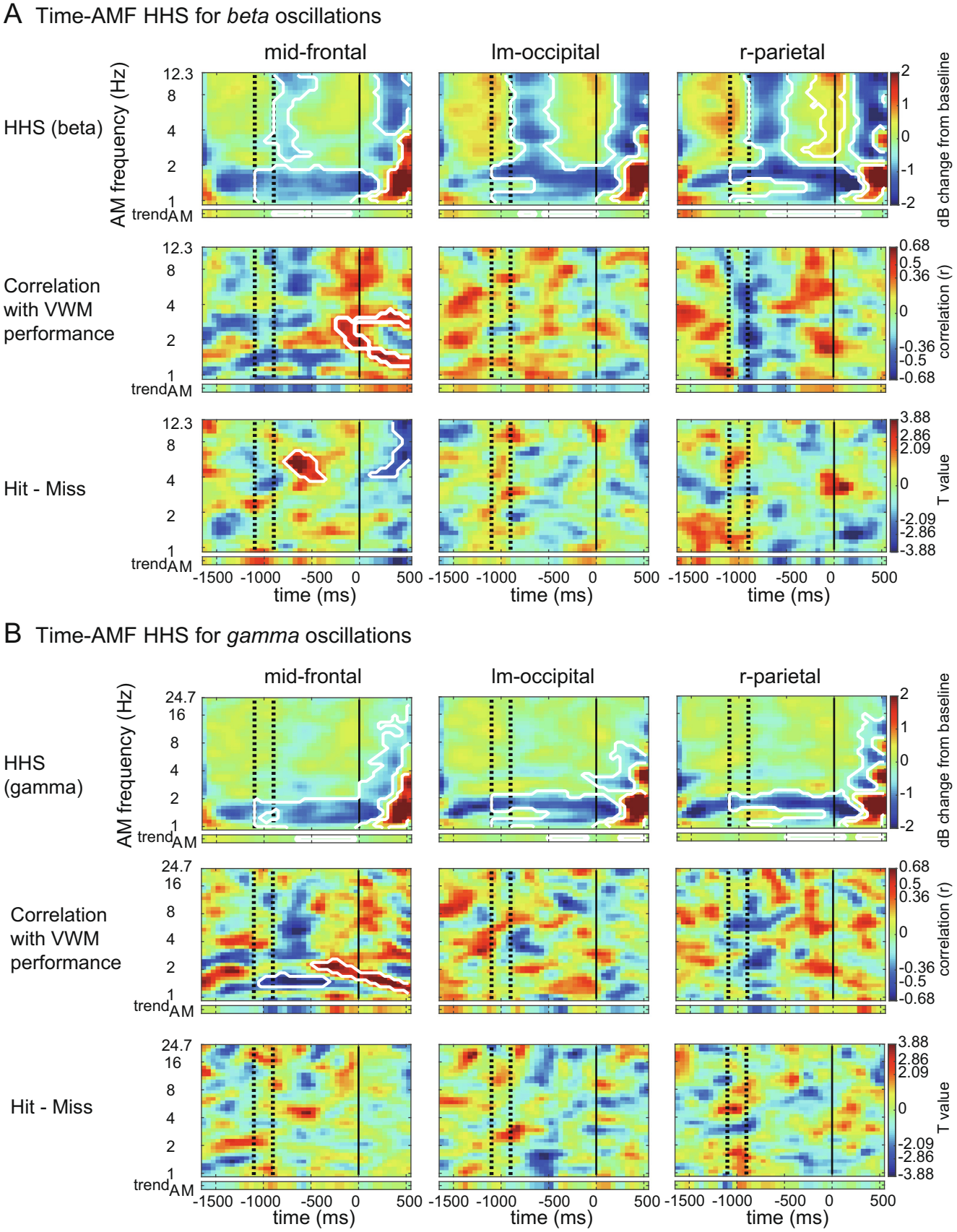
A Time-AMF HHS for beta oscillations
mid-frontal
lm-occipital
r-parietal
HHS (beta)
Correlation with VWM performance
Hit - Miss
AM frequency (Hz)
12.3
8
4
2
1
trendAM
dB change from baseline
correlation (r)
T value
2
1
0
-1
-2
0.68
0.5
0.36
-0.36
-0.5
-0.68
3.88
2.86
2.09
-2.09
-2.86
-3.88
-1500 -1000 -500 0 500
time (ms)
B Time-AMF HHS for gamma oscillations
HHS (gamma)
24.7
16

K = 2.27; SD = 0.78) and high-performing (N = 10; mean K = 4.64; SD = 0.60) group according to their VWM performance from the sham condition. Comparing to the global pattern of the two-phase desynchronization in the time-AMF HHS of *mid-frontal beta* AMs shown in Fig. 3A, the low- and high-performing groups showed different temporal dynamics of synchronization/desynchronization with AM frequencies above 2 Hz (Fig. 4A, top, first and second graphs): low performers showed a more pronounced second AM desynchronization during VWM *retrieval*, while high performers showed higher AM from the late VWM maintenance to early retrieval, as revealed by a two-sample CBnPP test between the high- and low-performing group (Fig. 4A, top, third graph). The significant differences were more pronounced in a region (cluster p = 0.024, max t = 3.83) that was partially overlapped with the result from the correlation analysis shown in Fig. 3A. In addition, in the r-parietal beta AMs, although both low- and high-performing groups maintained the pattern of the two-phase desynchronization, an additional (and significant) pattern of synchronization was observed during the late maintenance stage only in the high-performing group (Fig. 4A, bottom, second graph). We further investigated the contrast between the Hit and Miss conditions for the time-AMF HHS of *beta* oscillations in the low- and high-performing group separately. In the low-performing group, the power of mid-frontal beta AMs is significantly lower during VWM retrieval in Hit than Miss trials (SI Fig. S3A, top, first graph), suggesting that for low performers the second desynchronization is critical for a successful VWM. Furthermore, for high performers, the power of *r-parietal beta* AMs with AM frequency 3–5 Hz from the late maintenance to retrieval stage is significantly higher in Hit than Miss trials (SI Fig. S3A, bottom, second graph), implying that in the high performing group the r-parietal brain area was more involved in achieving successful VWM.

Findings from gamma AMs were similar to those from beta AMs. In both mid-frontal and r-parietal gamma AMs, low performers showed clear desynchronization of AM power in AM frequency 2–9 Hz during VWM retrieval, whereas high performers did not clearly exhibit this AM pattern (Fig. 4B, top, first and second graphs). The tendencies of the differences between the high- and low- performing group (Fig. 4B, from top to bottom, third graph) are consistent with the results from beta oscillations (shown in Fig. 4A), but the effects are not identified as significant under the two-sample CBnPP tests. Moreover, we investigated the contrast between the Hit and Miss conditions for the time-AMF HHS of gamma oscillations in the low- and high-performing group separately (SI Fig. S3B). Again, the tendency of clear Hit-Miss contrast in r-parietal gamma AMs for high performers is similar to beta AMs (shown in SI Fig. S3A), but not statistically significant.

Individual variability in anodal-tDCS responsiveness is determined by AMs in mid-frontal beta oscillations

Our behavioral results here and from previous studies have consistently shown that anodal-tDCS over rPPC is facilitative for low performers, but not helpful for the high performers (Tseng et al., 2012, 2016, 2018; Hsu et al., 2016). To look for the oscillatory neural correlates of such individual variability, we first performed a correlation analysis between the *change* (i.e. anodal-tDCS – sham) in the time-AMF HHS of beta oscillations and the behavioral change in the VWM performance induced by anodal tDCS. The *mid-frontal beta* AMs presented a pronounced cluster of positive correlation (cluster p = 0.038; peak r = 0.67) with the *change* of VWM performance, as shown in the Fig. 5A (top, first graph). Interestingly, the region of the pronounced correlation was within the AM frequency 2.6–4 Hz, from 150 ms before to 350 ms after the test array onset (i.e., from late maintenance to early retrieval). This region also partially overlapped with the region of pronounced correlation between mid-frontal beta AMs and the VWM performance in the sham condition (see Fig. 3A). This indicates that the mid-frontal beta AMs revealed in the critical ‘‘time-AMF” region may be one of the oscillatory neural correlates of tDCS efficacy and responsiveness. No significant correlation was found for l-/r-parietal beta AMs vs VWM performance, where, as shown in the Fig. 5A (middle and bottom row, first graph).

To further validate the observation above, we tested whether the beta AMs were affected differently by anodal tDCS between the low- and high-performing group. Consistent with the facilitative behavioral effect in the low-performing group, their power of *mid-frontal beta* AMs is greater in the anodal-tDCS compared to the sham condition (Fig. 5A, top, third graph; cluster p = 0.040, peak t = 5.21), and is found to be more pronounced within a time-AMF region that is partially overlapped with the region identified by the correlation analysis above (see Fig. 5A, top, first graph). This was not found in the high-performing group (Fig. 5A, top, second graph), which is also consistent with their behavioral data. For gamma oscillations, all the

Fig. 3. Temporal dynamics of AMs on beta and gamma brain oscillations. **(A)** Time-AMF HHS for the mid-frontal, lm-occipital, and r-parietal *beta* AMs (top, from left to right graphs), together with their correlation with VWM performance (middle, from left to right) and their Hit-Miss contrasts (bottom, from left to right). The correlation analyses indicate a significant correlation between the mid-frontal beta AMs and participants' VWM performance (highlighted by white contour) initiated from late VWM maintenance with AM frequency 2–4 Hz, followed by two ranges of AM frequencies (i.e. 1.5–2 and 3–4 Hz) during VWM retrieval (cluster p = 0.01, peak r = 0.66). **(B)** Time-AMF HHS for the mid-frontal, lm-occipital, and r-parietal *gamma* AMs, with conventions being the same as in **(A)**. The correlation analyses demonstrated the mid-frontal gamma AMs within AM frequencies from 1.5 to 2 Hz was first negatively correlated with the VWM performance during memory encoding and early maintenance, then positively correlated with the VWM performance during the late maintenance and retrieval stage (cluster p = 0.029, and 0.01).

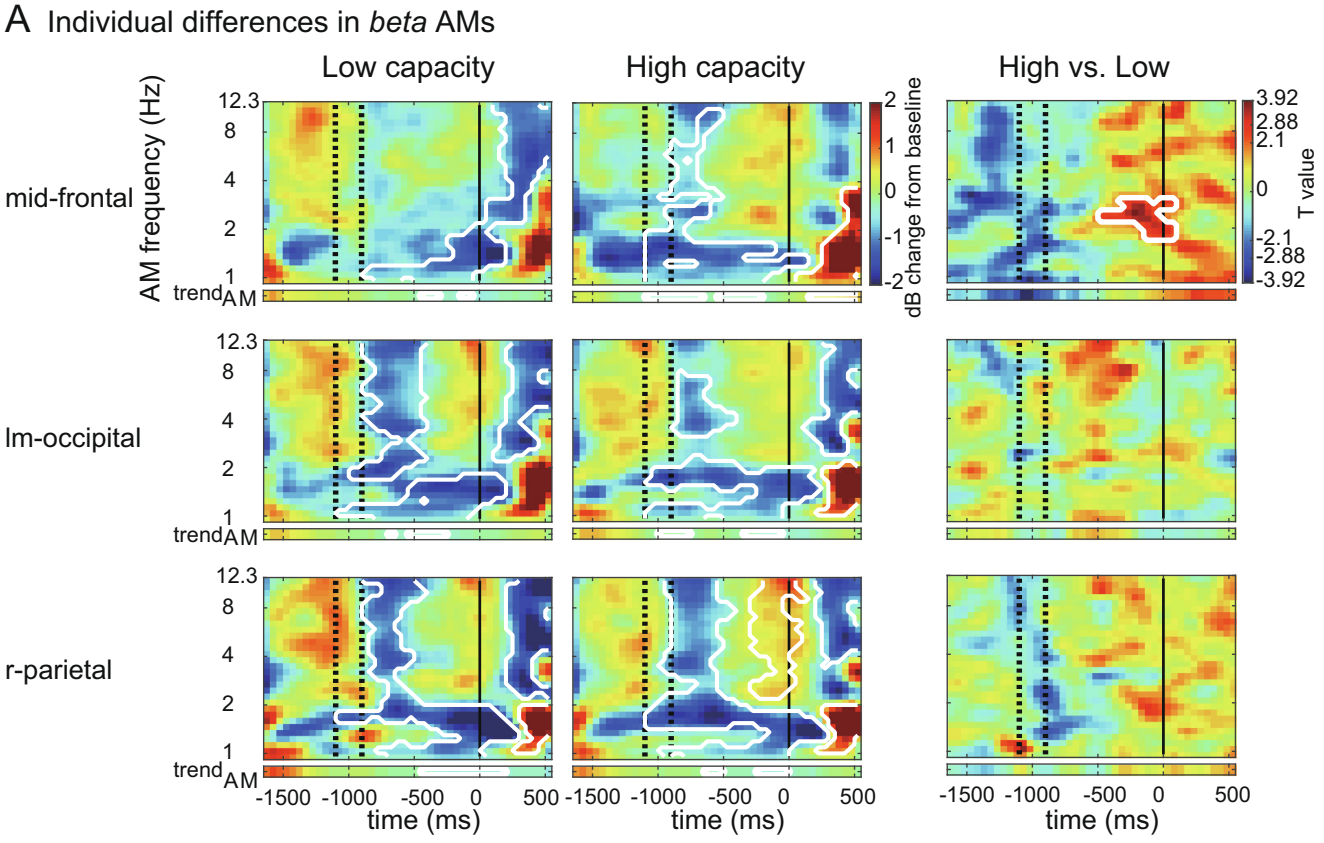
A Individual differences in beta AMs
Low capacity
High capacity
High vs. Low
mid-frontal
lm-occipital
r-parietal
AM frequency (Hz)
12.3
8
4
2
1
trend AM
dB change from baseline
2
1
0
-1
-2
T value
3.92
2.88
2.1
0
-2.1
-2.88
-3.92
-1500 -1000 -500 0 500
time (ms)

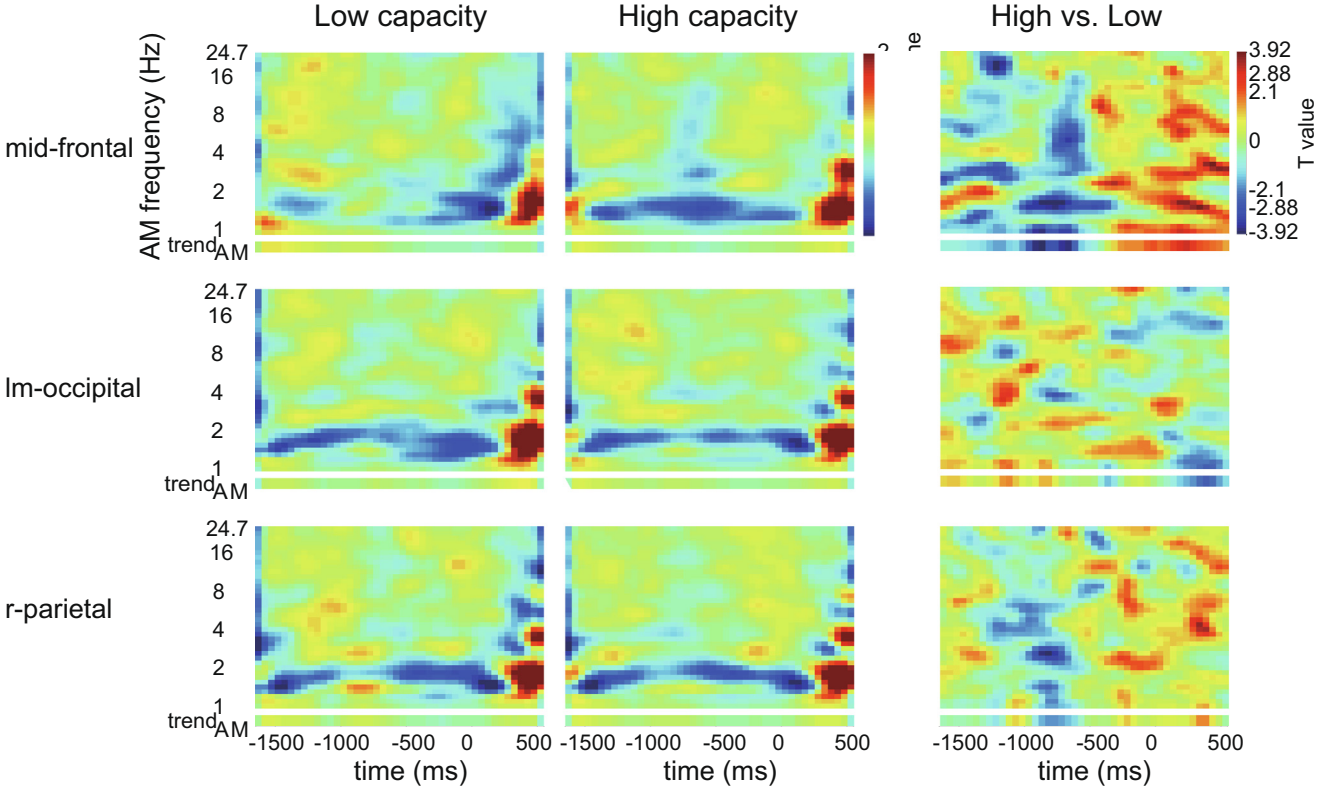
B Individual differences in gamma AMs
Low capacity
High capacity
High vs. Low
mid-frontal
lm-occipital
r-parietal
AM frequency (Hz)
24.7
16
8
4
2
1
trend AM
T value
3.92
2.88
2.1
0
-2.1
-2.88
-3.92
-1500 -1000 -500 0 500
time (ms)

analyses were the same as those for beta oscillations, but no significant correlation/effect was found (Fig. 5B). This suggests that anodal tDCS was primarily targeting beta AMs, and especially in the low-performing group to compensate for their lack of AMs from the stage of late maintenance to VWM retrieval. As a result, after anodal tDCS, the differences in mid-frontal beta AMs between the high- and low-performing groups were also reduced, as shown in Fig. 5C.

Together, changes in mid-frontal beta AMs that is induced by anodal rPPC tDCS seems to imply that there exists a mechanism for ‘‘inter-site” modulation during VWM processing. Our further hypothesis is that in VWM this inter-site modulating mechanism on beta/gamma AMs is underpinned by CFCs, with phases of a low-frequency (i.e., theta oscillation) modulating wave.

Local/long-range coupling between theta phase and beta/gamma AM in VWM

So far our HHS data have implied that (1) VWM-related AMs are supported by a local/long-range CFC mechanism, and (2) there exists a mechanism for inter-site anodal tDCS effect on beta AMs. Yet, there is a need to clearly measure this inter-site modulating mechanism of CFC. To investigate whether *theta* phase is a modulating source of the observed *beta/gamma* AM, we performed the HHCFPC analysis between theta phase and beta/gamma AM both from the perspective of local organization (i.e., when both theta phase and beta/gamma AM are measured at a single site) and long-range connectivity (i.e., from different sites). This HHCFPC analysis consisted of 9 couplings among all the bivariate arrangements out of the mid-frontal, lm-occipital, and r-parietal ICs: 3 local and 6 long-range directional couplings. These couplings were represented as elements in a connectivity matrix, with their corresponding graph form in Fig. 6A (bottom, second graph). In this study HHCFPC was computed with 600-ms time segments and 100-ms sliding steps, which allowed approximately 3 theta cycles (see the ‘‘5 Hz” peak frequency of the frequency distribution of IMF 5 shown in Fig. 6A, first graph on the bottom).

We first analyzed HHCFPC between *theta* phase and *beta* AM. Top two panels of Fig. 6B show the grand averaged HHCFPC in the sham condition, together with their correlations with VWM performance. The averaged phase locking values (PLVs) among these couplings ranged from 0.47 to 0.60. The correlation analysis between HHCFPC and VWM performance reveals that the pronounced correlation (fully opaque colors; cluster $p = 0.025$, peak $r = 0.80$) consisted of a pair of couplings from (1) mid-frontal theta phase to r-parietal beta AM through the middle and late maintenance stage, and (2) reciprocally from r-parietal theta phase to mid-frontal beta AM during the middle maintenance stage, as well as local couplings both in the (3) mid-frontal and (4) r-parietal ICs for the period of late maintenance, and a coupling from (5) r-parietal theta phase to lm-occipital beta AM that appeared in the late maintenance stage, and crossed over to the retrieval stage.

We then tested whether individual differences in anodal-tDCS efficacy/responsiveness may have been a result of one (or more) of these couplings. To this end, we performed the CBnPP test to compare HHCFPC between the anodal-tDCS and sham conditions within the low- and high-performing group (Fig. 6B, middle two panels). For low performers, the test revealed significantly enhanced theta phase-beta AM couplings from anodal-tDCS, which was more prominent from r-parietal to mid-frontal, from r-parietal to lm-occipital, and local lm-occipital -to- lm-occipital (fully opaque colors; cluster $p = 0.033$, peak $t = 3.9$), with the first two being consistent with the VWM-correlated couplings identified above. This result not only explains the anodal-tDCS facilitating effect on VWM in the low performing group from the perspective of long-range cross-frequency coupling, but also demonstrates how anodal-tDCS effect *propagates* from r-parietal to mid-frontal brain areas by means of theta-beta CFC, thereby enhancing AMs in mid-frontal beta oscillations. In contrast, for high performers, the test indicated that anodal-tDCS did not enhance the theta-beta CFC, which is consistent with the behavior results.

We next analyzed HHCFPC between *theta* phase and *gamma* AM. Top two panels of Fig. 6C depict the grand averaged HHCFPC and their correlations with VWM performance. A robust correlation (cluster $p = 0.009$, peak $r = 0.75$) was found to include (1) a coupling started in encoding and ended in early maintenance stage from mid-frontal theta phase to lm-occipital gamma AM, (2) a coupling started in encoding but continued to the end of retrieval stage from mid-frontal theta phase to r-parietal gamma AM, (3) a coupling that appeared transiently in maintenance stage from r-

Fig. 4. Individual differences in VWM performance are revealed by beta and gamma AMs. **(A)** Low- and high-performing groups' time-AMF HHS for the mid-frontal, lm-occipital, and r-parietal *beta* AMs, and a comparison of beta AMs between both groups (two-sample CBnPP test). Low performers showed a more pronounced second AM desynchronization during VWM retrieval, while high performers showed higher AM from the late VWM maintenance to early retrieval, as revealed by a two-sample CBnPP test between the high- and low-performing groups (top, third graph; cluster $p = 0.024$, max $t = 3.83$). **(B)** Similar to **(A)**, but for *gamma* AMs. Low performers showed clear desynchronization of AM power in AM frequency 2–9 Hz during VWM retrieval, whereas the high performers did not clearly exhibit this AM pattern. The tendencies of the comparison between high- and low-performing group are consistent with the results from beta oscillations, but the effects are not identified as significant under the two-sample CBnPP tests.

A *Beta* oscillations: analysis of AMs between tDCS and sham

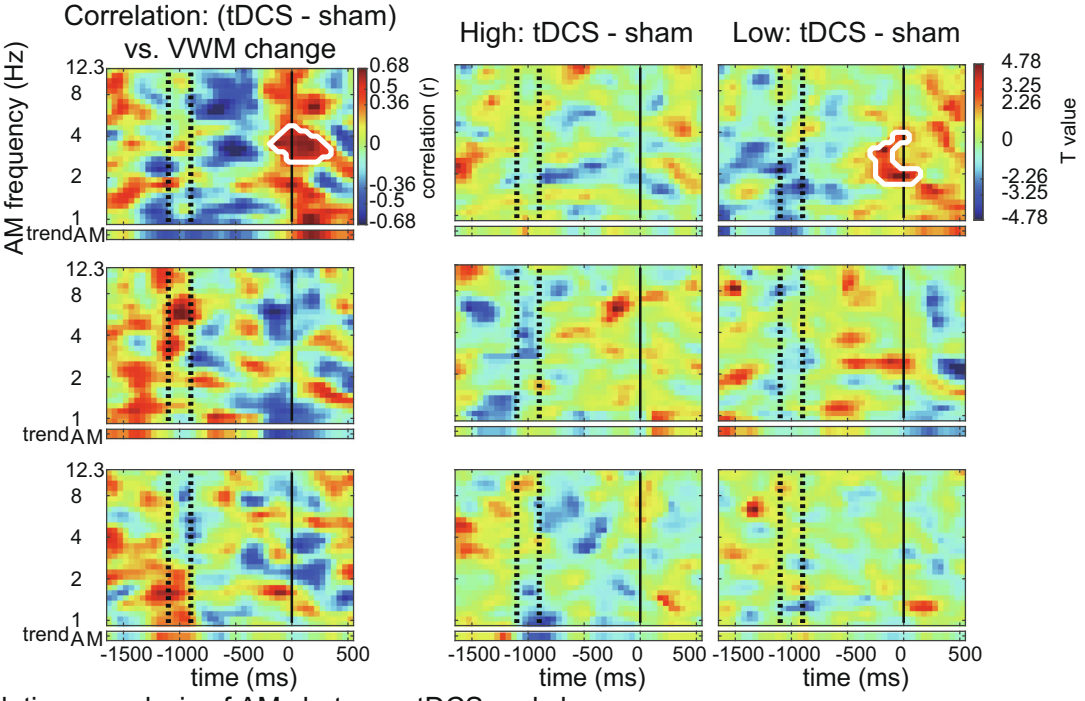

B *Gamma* oscillations: analysis of AMs between tDCS and sham

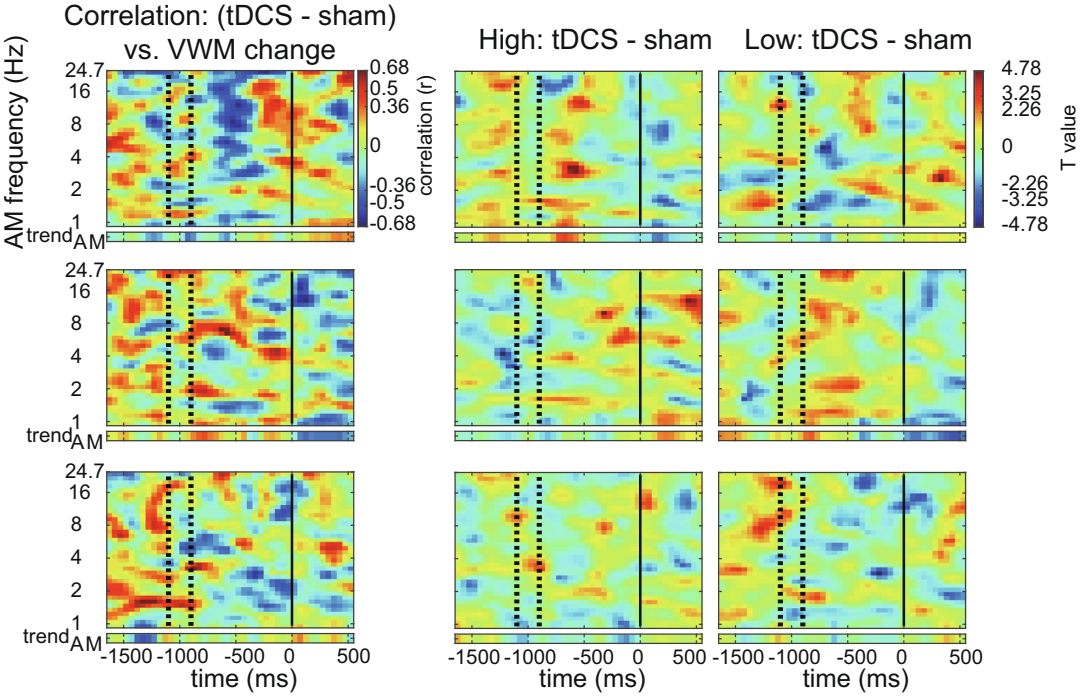

C Reduction of individual differences in mid-frontal beta AMs after anodal tDCS

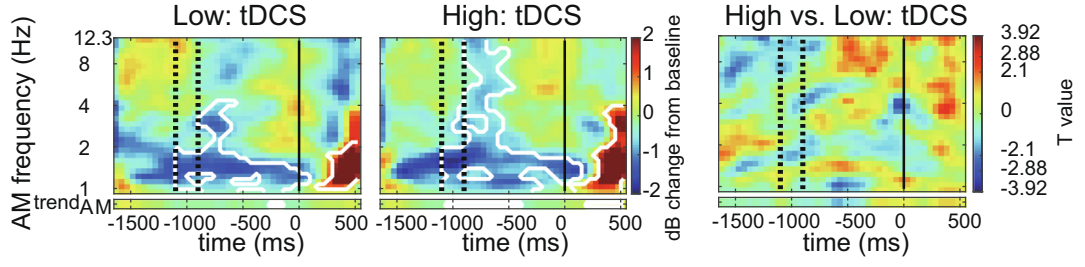

parietal theta phase to lm-occipital gamma AM, and (4) a local r-parietal coupling that appeared in the retrieval and comparison stage. Again, we tested whether individual differences in responsiveness to anodal-tDCS can be revealed by the HHCFPC between theta phase and gamma AM. However, in both low- and high- performing groups, we did not observe enhanced theta-gamma CFCs due to tDCS (Fig. 6C, middle two panels), implying that the present protocol of anodal-tDCS may have primarily targeted the theta-beta couplings during VWM processing.

Together, the above results highlight the importance of r-parietal (Gelastopoulos et al., 2019) and mid-frontal beta/gamma AMs in both or either the two ways: (1) based on their own AM power (as demonstrated in previous sections), and (2) based on their local and long-range CFCs with theta phase.

DISCUSSION

In this study we found that AM power of mid-frontal *beta* and *gamma* oscillations correlated with people's natural VWM performance, first in AM frequency 1.8–4 Hz during the late maintenance stage, and next in AM frequency 1.5–2 Hz (both in beta and gamma) and 3–4 Hz (only in beta) during the retrieval stage. When VWM was modulated via anodal-tDCS, changes in VWM capacity were tracked by the 2.6–4.4 Hz AM power changes in mid-frontal beta oscillations from the late maintenance to the early retrieval stage. Intra-/inter-site cross-frequency connectivity analysis indicated that the *theta* phase-*beta* AM bidirectional couplings, between r-parietal and mid-frontal brain areas (Woodman et al., 2003; Johnson et al., 2017) during VWM maintenance, are also associated with participants' natural VWM performance, thereby suggesting that the effects of mid-frontal *beta* AM found in the present study was related to r-parietal theta oscillation. Moreover, for the low-performing group, the strengthened coupling from r-parietal theta to mid-frontal beta AM in the anodal rPPC tDCS condition suggests that anodal tDCS can exert its facilitating effect via cross-frequency connectivity from the targeting site (i.e., r-parietal) to the linked site (i.e., mid-frontal), therefore resulting in an AM enhancement within a low theta-range AM frequency in mid-frontal beta oscillation and the correlated behavioral change in VWM performance. These results demonstrate a crucial role for AMs, as well as its propagation through different frontoparietal long-distance inter-sites, in supporting (and explaining individual differences in) VWM.

Previous research has identified CFC between frontal theta and posterior gamma oscillations as one of the fundamental neural correlates of VWM (Friese et al., 2013). The present study found that during VWM, frontal theta coupled not only with posterior gamma, but also with posterior beta oscillations. Moreover, we found that *right posterior theta* also coupled with *frontal beta* oscillations, thereby providing required modulating mechanism for mid-frontal beta AMs. Therefore, we propose that this bidirectional CFC between the mid-frontal and parietal brain regions (Johnson et al., 2017) plays a crucial role in VWM maintenance, and argue that the importance of parietal-to-frontal theta-beta coupling is nothing less than that of frontal-to-parietal CFCs. Direct evidence for this argument comes from the high-performing group's significantly-greater AM power within low-theta AM frequency in mid-frontal beta oscillation during the late VWM maintenance stage, over the low-performing group.

This means that better VWM representation is related to how mid-frontal beta is modulated by a "theta-modulating force" (i.e., theta-beta CFC). This argument is further supported by the causal evidence of anodal-tDCS over rPPC (Tseng et al., 2012), where both strengthened parietal-to-frontal theta-beta coupling and enhanced mid-frontal beta-AM were evident in the low-performing group that had benefited from the anodal-tDCS in VWM. Fig. 7A shows the dynamical change of AM power within a low theta-range AM frequency 1.8–4 Hz in mid-frontal beta oscillation. In the sham condition, following a common pattern of desynchronization in VWM encoding and early maintenance, a clear ascending phase of AM power continuing to the late maintenance stage was observed in the high-performing group, but not in the low-performing group. After anodal-tDCS, the ascending phase turned out to be marked in the low-performing group, while maintaining its original clear pattern in the high-performing group, both of which are consistent with the behavioral patterns in VWM. For low-performers, the indistinct/short ascending phase of mid-frontal beta-AM power may have been caused by a deficit in "theta-modulating force" from the r-parietal region, which is later strengthened by anodal-tDCS over rPPC, as shown in Fig. 7A.

Fig. 5. Individual variability in anodal-tDCS responsiveness is determined by AMs in *mid-frontal beta* oscillations. **(A)** Analysis of AMs in *beta* oscillations between tDCS and sham conditions. A correlation analysis between the change (i.e. anodal-tDCS – sham) of the time-AMF HHS of beta oscillations and the behavioral change of the VWM performance induced by anodal tDCS (from top to bottom rows, first graphs, for the mid-frontal, lm-occipital, and r-parietal *beta* AM, respectively) revealed that the mid-frontal beta AM was positively correlated with the change of VWM performance (cluster $p = 0.038$; peak $r = 0.67$). The contrast between tDCS and sham conditions was also investigated for high- and low-performing group separately (from top to bottom rows, second and third graphs, respectively). Consistent with the facilitative behavioral effect in the low-performing group, their power of mid-frontal beta AMs is greater in the anodal-tDCS compared to the sham condition (cluster $p = 0.040$, peak $t = 5.21$; see the right top graph). **(B)** Analysis of AMs in *gamma* oscillations between tDCS and sham conditions. For gamma oscillation all the analyses were the same as those for beta oscillations, but no significant correlation/effect was found. **(C)** Reduction of the differences in mid-frontal beta AMs between high- and low-performing groups after anodal tDCS.

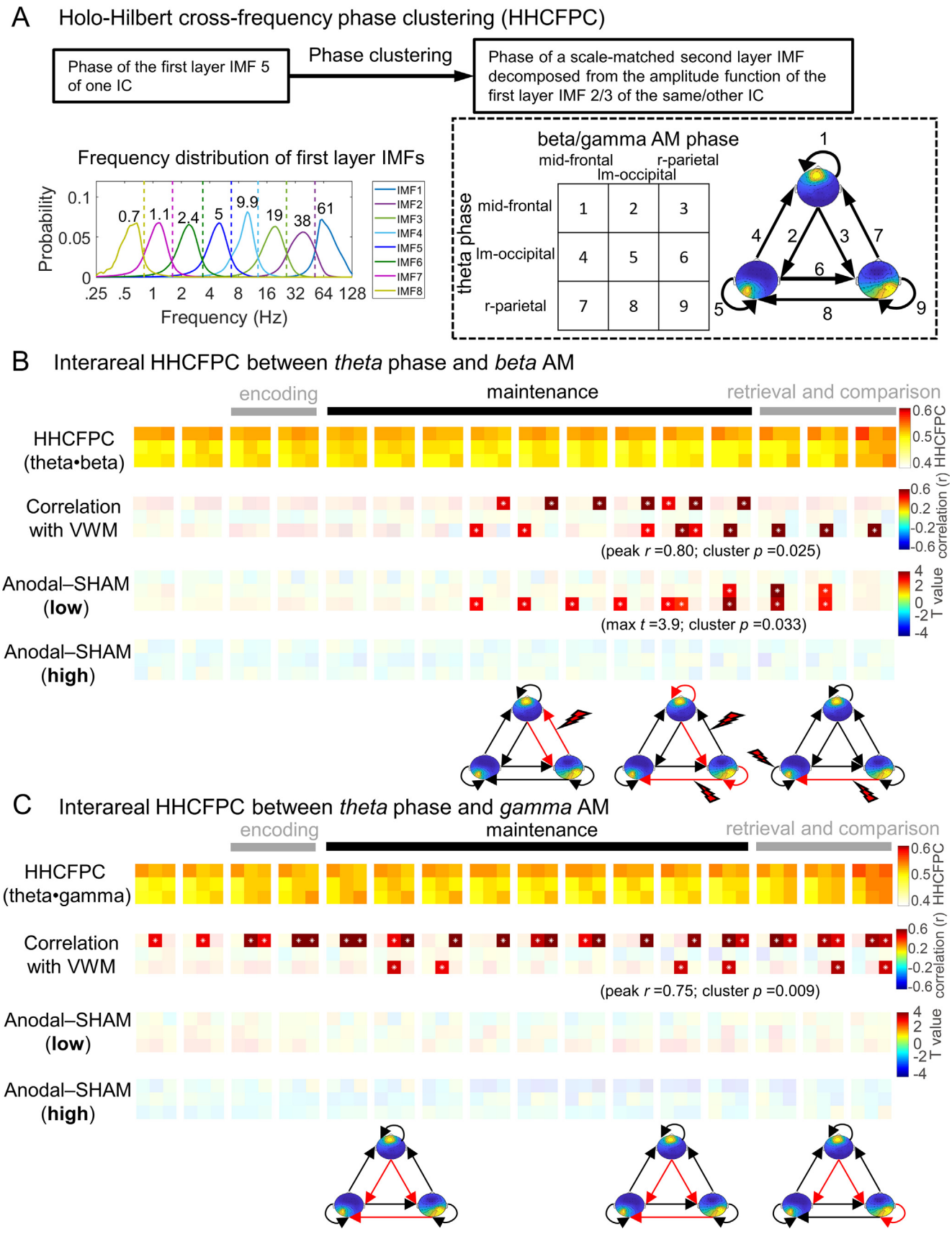
A
Holo-Hilbert cross-frequency phase clustering (HHCFPC)
Phase of the first layer IMF 5 of one IC
Phase clustering
Phase of a scale-matched second layer IMF decomposed from the amplitude function of the first layer IMF 2/3 of the same/other IC
Frequency distribution of first layer IMFs
Probability
0.1
0.05
0
0.7
1.1
2.4
5
9.9
19
38
61
.25 .5 1 2 4 8 16 32 64 128
Frequency (Hz)
IMF1
IMF2
IMF3
IMF4
IMF5
IMF6
IMF7
IMF8
beta/gamma AM phase
mid-frontal
r-parietal
lm-occipital
theta phase
mid-frontal
lm-occipital
r-parietal
1 2 3
4 5 6
7 8 9
1
2
3
4
5
6
7
8
9
B
Interareal HHCFPC between theta phase and beta AM
encoding
maintenance
retrieval and comparison
HHCFPC (theta•beta)
0.6
0.5
0.4
HHCFPC
Correlation with VWM
0.6
0.2
-0.2
-0.6
correlation (r)
(peak r =0.80; cluster p =0.025)
Anodal–SHAM (low)
4
2
0
-2
-4
T value
(max t =3.9; cluster p =0.033)
Anodal–SHAM (high)
C
Interareal HHCFPC between theta phase and gamma AM
encoding
maintenance
retrieval and comparison
HHCFPC (theta•gamma)
0.6
0.5
0.4
HHCFPC
Correlation with VWM
0.6
0.2
-0.2
-0.6
correlation (r)
(peak r =0.75; cluster p =0.009)
Anodal–SHAM (low)
4
2
0
-2
-4
T value
Anodal–SHAM (high)

Our data here can also be used to empirically test the predictions based on an oscillatory short-term memory buffer model (Lisman and Idiart, 1995; Jensen and Lisman, 1998; Lisman and Jensen, 2013). The model states that multiple items are transiently stored in WM via nesting fast (e.g., beta/gamma) oscillations into slower (e.g., theta) ones, predicting that the frequency of the slow modulating oscillation will adaptively decrease from the maintenance to retrieval stage to achieve a successful WM. Therefore, the number of high-frequency cycles that can be nested into each theta cycle along with its adaptive change become one of the determining factors of VWM capacity. In HHSA, with the aid of its two-layer scheme of IMF and instantaneous frequency, the adaptive dynamical change of the scale of nested beta/gamma can be investigated by looking into the variation of instantaneous AM frequency in the theta-scale-matched second-layer IMF. Following this idea, if we take beta- (IMF 3; Fig. 7B, left panel) and gamma-related (IMF 2; Fig. 7B, right panel) first-layer IMF and extract theta-scale-matched second-layer IMF, then averaged theta-range AM frequency during the retrieval stage (1–500 ms) would be negatively correlated with participants' VWM capacity (beta: $r = -0.511$, $p = 0.021$; gamma: $r = -0.445$, $p = 0.049$). Furthermore, when we compared the theta-range AM frequency from the retrieval stage with that from the early maintenance (first 400-ms) stage to see whether it would adaptively decrease along the VWM process, we observed that (1) for beta oscillation, the decrease in theta-range AM frequency was only significant in high performers ($p = 0.037$; Fig. 7C, left panel); and (2) for gamma oscillation, the effect was observed in both low and high performers (low: $p < 0.001$, high: $p = 0.002$; Fig. 7C, right panel). These results not only provide evidence to the oscillatory WM buffer model, but also explain why pronounced correlation between mid-frontal beta/gamma AMs and VWM performance would occur at the lower bound of the theta-range AM frequency (~2–4 Hz), i.e., VWM benefited from this lowered AM frequency (Vosskuhl et al., 2015; Turi et al., 2018; Wolinski et al., 2018; Bender et al., 2019). A schematic representation of the results above on theta-range AM frequency as periodic wave packets is illustrated in Fig. 7D.

The results of this study may imply that VWM can also be modulated by noninvasive brain stimulations (NIBSs) [e.g., tDCS, transcranial alternative current stimulation (tACS) (Herrmann et al., 2013; Helfrich et al., 2014), and amplitude modulated tACS (AM-tACS) (Witkowski et al., 2016; Negahbani et al., 2018)] over the mid-frontal brain area. However, previous studies have demonstrated that simply delivering NIBSs over the mid-frontal brain region may be difficult to induce facilitating effect on VWM performance (Witkowski et al., 2016; Negahbani et al., 2018). Therefore, according to the HHCFPC results in this study, further studies are expected to strengthen the intersite CFCs within the frontoparietal system through using AM-tACS (e.g., carrier frequency: beta; envelope frequency: theta) over the mid-frontal brain area, in conjunction with theta-tACS over the r-parietal brain region, or vice versa.

Taken together, we employed HHSA, HHCFPC, and tDCS to unveil the importance of mid-frontal beta AM and its interareal coupling with r-parietal theta phase for VWM maintenance and retrieval. We further revealed that for VWM maintenance the significance of parietal beta/gamma AM is primarily driven by its coupling with mid-frontal theta. Finally, we demonstrated that the dynamical power change of mid-frontal beta AM not only tracked individual differences of participants' VWM capacity, but also their tDCS responsiveness/efficacy.

LIMITATIONS

For the correlation analyses between the behavioral and neurophysiological data in this study, the required sample size was estimated to be 19 in an a priori power analysis (see *Participants* in Experimental procedures). Therefore, the sample size of 20 used in this study should be sufficient to support the correlation analyses between the HHS/ HHCFPC and behavioral data. However, when participants were divided into a high-performing and low-performing group, statistical results in both behavioral and HHS/HHCFPC data were limited by the small sample size of 10 for each group. The desired sample size of each of the two groups is 26 for two-sample *t*-tests, estimated by an a priori power analysis with the expected effect size (Cohen's *d*) of 0.8 under the criteria $\alpha = 0.05$ (two-tailed) and $\beta = 0.2$. On the other hand, for the within-subjects tDCS effect on each group, the anticipated sample size is 18 with parameters the same as above (i.e., d = 0.8, $\alpha = 0.05$, $\beta = 0.2$).

FUNDING

This work was supported by the Ministry of Science and Technology, Taiwan, ROC (grant numbers: 106-2410-H-008-038-MY3; 104-2420-H-008-003-MY2; 108-2639-H-

Fig. 6. Local/long-range couplings between *theta* phase and *beta/gamma* AM in VWM. **(A)** Schematic illustration of the Holo-Hilbert cross-frequency phase clustering (HHCFPC) analysis. HHCFPC in this study was achieved by clustering phase angle differences between theta phase (i.e., the instantaneous phase of the first layer IMF 5) and a series of phase data corresponding to a "scale-matched" IMF obtained by decomposing the amplitude function (i.e. an IMF obtained from the second layer EMD, with its instantaneous AM frequency closest to the theta range) of beta/gamma (i.e., IMF 3/2) oscillations. The HHCFPC consisted of 9 couplings among all the bivariate arrangements out of the mid-frontal, lm-occipital, and r-parietal ICs, represented as a connectivity matrix, with their correspondence to a graph form (bottom panel). **(B)** HHCFPC between *theta* phase and *beta* AM. The top two panels showed the grand averaged HHCFPC in the sham condition, together with their correlations with VWM performance. Pronounced connections were shown in fully opaque colors with asterisks. Middle two panels demonstrated the statistical contrast of HHCFPC between the anodal-tDCS and sham conditions within the low- and high-performing group, respectively. The correlated connections and low performers' tDCS effects are also demonstrated as red directional arrows and thunder sign, respectively, on the bottom panel. **(C)** HHCFPC between *theta* phase and *gamma* AM. Conventions are the same as in **(B)**. (For interpretation of the references to colour in this figure legend, the reader is referred to the web version of this article.)

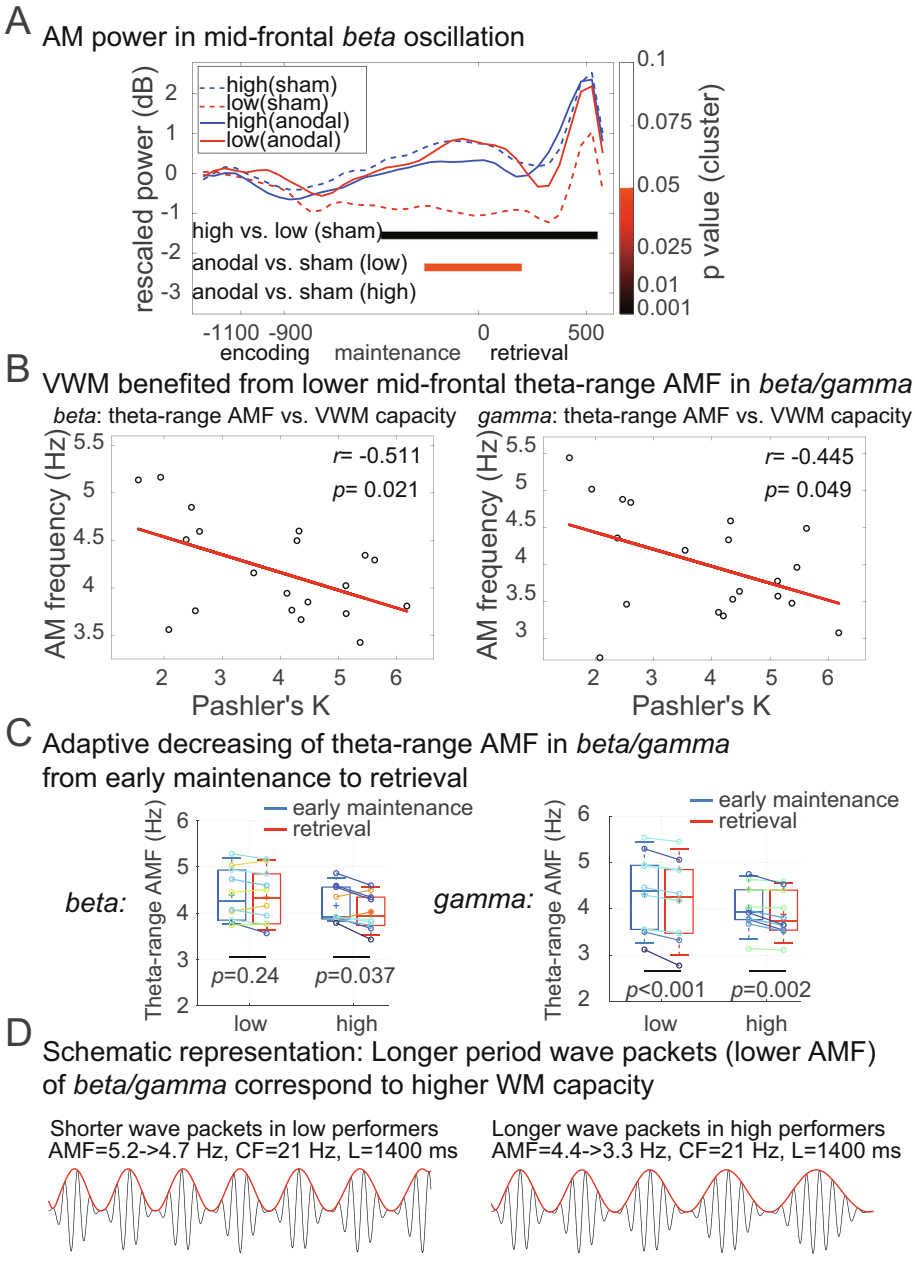

Fig. 7. Evidence of *beta/gamma* AMs as brain oscillatory correlates for VWM. **(A)** Dynamical change of AM power within low theta-range AM frequency in mid-frontal beta oscillation tracks the VWM performance. In the sham condition (dotted), following a common attenuated pattern during VWM encoding and early maintenance, a clear ascending phase of AM power continuing to the late maintenance stage was observed in the high-performing group (blue), but not in the low-performing group (red). After anodal-tDCS (solid), the ascending phase turned out to be distinct in the low-performing group, but remained its original clear pattern in the high-performing group, consistent with the behavioral change of VWM by the anodal-tDCS. **(B)** VWM capacity is negatively correlated with the mid-frontal theta-range AM frequency in beta ($r = -0.511$; $p = 0.021$; $N = 20$) and gamma ($r = -0.445$; $p = 0.049$) oscillations. This is based on an oscillatory short-term memory buffer model that suggests the adaptive change of the number of high-frequency cycles nested in each theta cycle is related to VWM performance. **(C)** Adaptive decreasing of theta-range AM frequency in *beta* and *gamma* oscillations across early WM maintenance to retrieval stage (shown by box-and-whisker plots, where the box depicts the median and the 25th and 75th quartiles and the whisker shows the 5th and 95th percentile). **(D)** Schematic illustration of adaptive theta-range AM frequency of beta/gamma oscillation, where wave packets with a longer and adaptive period (right panel) are related to higher performance in VWM. (For interpretation of the references to colour in this figure legend, the reader is referred to the web version of this article.)

008-001-ASP; 108-2321-B-075-004-MY2; 108-2410-H-038-009; 109-2423-H-038-001-MY4); Academia Sinica, Taiwan (AS-108-TP-C02-2) and also sponsored by Taiwan Ministry of Education's "Academic Strategic Alliance: Taiwan and Oxford University" project grant (MOE Oxford-NCU-BRC collaborative project).

CONFLICT OF INTEREST

No.

AUTHOR CONTRIBUTIONS

W.K.L., P.T., C.H.J., designed the experiments and collected the data. W.K.L., J. R. Y., N.E.H. analyzed data. All authors wrote the manuscript.

ACKNOWLEDGEMENTS

We would like to express our gratitude to Drs Neil Muggleton, Kia Nobre, Mark Woolrich, Freek van Ede, and Andrew Quinn for their insightful comments on earlier versions of this paper.

DECLARATIONS OF INTEREST

None.

REFERENCES

Antal A, Alekseichuk I, Bikson M, Brockmöller J, Brunoni AR, Chen R, Cohen L, Dowthwaite G, Ellrich J, Flöel A (2017) Low intensity transcranial electric stimulation: safety, ethical, legal regulatory and application guidelines. Clin Neurophysiol 128:1774–1809.

Aru J, Aru J, Priesemann V, Wibral M, Lana L, Pipa G, Singer W, Vicente R (2015) Untangling cross-frequency coupling in neuroscience. Curr Opin Neurobiol 31:51–61.

Axmacher N, Henseler MM, Jensen O, Weinreich I, Elger CE, Fell J (2010) Cross-frequency coupling supports multi-item working memory in the human hippocampus. Proc Natl Acad Sci 107:3228–3233.

Bell AJ, Sejnowski TJ (1995) An information-maximization approach to blind separation and blind deconvolution. Neural Comput 7:1129–1159.

Bender M, Romei V, Sauseng P (2019) Slow theta tACS of the right parietal cortex enhances contralateral visual working memory capacity. Brain Topogr 32:477–481.

Bikson M, Grossman P, Thomas C, Zannou AL, Jiang J, Adnan T, Mourdoukoutas AP, Kronberg G, Truong D, Boggio P (2016) Safety of transcranial direct current stimulation: evidence based update 2016. Brain Stimulation 9:641–661.

Canolty RT, Knight RT (2010) The functional role of cross-frequency coupling. Trends Cognit Sci 14:506–515.

Cavanagh JF, Frank MJ (2014) Frontal theta as a mechanism for cognitive control. Trends Cognit Sci 18:414–421.

Chuang K-Y, Chen Y-H, Balachandran P, Liang W-K, Juan C-H (2019) Revealing the electrophysiological correlates of working memory-load effects in symmetry span task with HHT method. Front Psychol 10.

Cohen MX (2014) Analyzing neural time series data: theory and practice. Cambridge, Massachusetts: The MIT Press.

Daume J, Gruber T, Engel AK, Friese U (2017) Phase-amplitude coupling and long-range phase synchronization reveal frontotemporal interactions during visual working memory. J Neurosci 37:313–322.

Deering R, Kaiser JF., 2005. The use of a masking signal to improve empirical mode decomposition. Proceedings (ICASSP'05). IEEE International Conference on Acoustics, Speech, and Signal Processing, 2005. IEEE, pp. iv/485-iv/488 Vol. 484.

Delorme A, Makeig S (2004) EEGLAB: an open source toolbox for analysis of single-trial EEG dynamics including independent component analysis. J Neurosci Methods 134:9–21.

Delorme A, Palmer J, Onton J, Oostenveld R, Makeig S (2012) Independent EEG sources are dipolar. PLoS ONE 7.

Fell J, Axmacher N (2011) The role of phase synchronization in memory processes. Nat Rev Neurosci 12:105–118.

Friese U, Koster M, Hassler U, Martens U, Trujillo-Barreto N, Gruber T (2013) Successful memory encoding is associated with increased cross-frequency coupling between frontal theta and posterior gamma oscillations in human scalp-recorded EEG. Neuroimage 66:642–647.

Gelastopoulos A, Whittington MA, Kopell NJ (2019) Parietal low beta rhythm provides a dynamical substrate for a working memory buffer. PNAS 116:16613–16620.

Groppe DM, Urbach TP, Kutas M (2011) Mass univariate analysis of event-related brain potentials/fields I: a critical tutorial review. Psychophysiology 48:1711–1725.

Hanslmayr S, Aslan A, Staudigl T, Klimesch W, Herrmann CS, Bauml KH (2007) Prestimulus oscillations predict between and within subjects. Neuroimage 37:1465–1473.

Hanslmayr S, Staudigl T (2014) How brain oscillations form memories—a processing based perspective on oscillatory subsequent memory effects. NeuroImage 85:648–655.

Helfrich RF, Knight RT (2016) Oscillatory dynamics of prefrontal cognitive control. Trends Cognit Sci 20:916–930.

Helfrich RF, Schneider TR, Rach S, Trautmann-Lengsfeld SA, Engel AK, Herrmann CS (2014) Entrainment of brain oscillations by transcranial alternating current stimulation. Curr Biol 24:333–339.

Herrmann CS, Rach S, Neuling T, Strüber D (2013) Transcranial alternating current stimulation: a review of the underlying mechanisms and modulation of cognitive processes. Front Hum Neurosci 7:279.

Hsu T-Y, Juan C-H, Tseng P (2016) Individual differences and state-dependent responses in transcranial direct current stimulation. Front Hum Neurosci 10:643.

Hsu TY, Tseng P, Liang WK, Cheng SK, Juan CH (2014) Transcranial direct current stimulation over right posterior parietal cortex changes prestimulus alpha oscillation in visual short-term memory task. Neuroimage 98:306–313.

Huang NE, Hu K, Yang ACC, Chang HC, Jia D, Liang WK, Yeh JR, Kao CL, Juan CH, Peng CK, Meijer JH, Wang YH, Long SR, Wu ZH (2016) On Holo-Hilbert spectral analysis: a full informational spectral representation for nonlinear and non-stationary data. Philos Trans Royal Soc - Math Phys Eng Sci 374:20150206.

Huang NE, Shen Z, Long SR, Wu MLC, Shih HH, Zheng QN, Yen NC, Tung CC, Liu HH (1998) The empirical mode decomposition and the Hilbert spectrum for nonlinear and non-stationary time series analysis. Proc Royal Soc - Math Phys Eng Sci 454:903–995.

Huang NE, Wu Z, Long SR, Arnold KC, Chen X, Blank K (2009) On instantaneous frequency. Adv Adapt Data Anal 1:177–229.

Hulley SB, Cummings SR, Browner WS, Grady D, Newman TB. 2007. Designing clinical research. 3rd ed. Appendix 6C, 3rd edition ed. Wolters Kluwer/Lippincott Williams & Wilkins, Philadelphia.

Hyvarinen A (2011) Testing the ICA mixing matrix based on inter-subject or inter-session consistency. Neuroimage 58:122–136.

Hyvarinen A, Oja E (2000) Independent component analysis: algorithms and applications. Neural Networks 13:411–430.

Hyvarinen A, Ramkumar P (2013) Testing independent component patterns by inter-subject or inter-session consistency. Front Hum Neurosci 7.

Jaiswal S, Tsai SY, Juan CH, Muggleton NG, Liang WK (2019) Low delta and high alpha power are associated with better conflict control and working memory in high mindfulness, low anxiety individuals. Social Cognit Affect Neurosci 14:645–655.

Jensen O, Lisman JE (1998) An oscillatory short-term memory buffer model can account for data on the Sternberg task. J Neurosci 18:10688–10699.

Johnson EL, Dewar CD, Solbakk AK, Endestad T, Meling TR, Knight RT (2017) Bidirectional frontoparietal oscillatory systems support working memory. Curr Biol 27:1829.
Lachaux JP, Rodriguez E, Martinerie J, Varela FJ (1999) Measuring phase synchrony in brain signals. Hum Brain Mapp 8:194–208.
Lisman JE, Idiart MAP (1995) Storage of 7 + /-2 short-term memories in oscillatory subcycles. Science 267:1512–1515.
Lisman JE, Jensen O (2013) The theta-gamma neural code. Neuron 77:1002–1016.
Lopes-dos-Santos V, van de Ven GM, Morley A, Trouche S, Campo-Urriza N, Dupret D (2018) Parsing hippocampal theta oscillations by nested spectral components during spatial exploration and memory-guided behavior. Neuron 100 940-952.e947.
Luck SJ, Vogel EK (1997) The capacity of visual working memory for features and conjunctions. Nature 390:279–281.
Makeig S, AnlloVento L, Jung P, Bell AJ, Sejnowski TJ, Hillyard SA (1996) Independent component analysis of event-related potentials during a selective attention task. Psychophysiology 33:S58.
Makeig S, Debener S, Onton J, Delorme A (2004) Mining event-related brain dynamics. Trends Cognit Sci 8:204–210.
Maris E, Oostenveld R (2007) Nonparametric statistical testing of EEG- and MEG-data. J Neurosci Methods 164:177–190.
Negahbani E, Kasten FH, Herrmann CS, Fröhlich F (2018) Targeting alpha-band oscillations in a cortical model with amplitude-modulated high-frequency transcranial electric stimulation. Neuroimage 173:3–12.
Nguyen KT, Liang WK, Lee V, Chang WS, Muggleton NG, Yeh JR, Huang NE, Juan CH (2019) Unraveling nonlinear electrophysiologic processes in the human visual system with full dimension spectral analysis. Sci Rep 9.
Nitsche MA, Cohen LG, Wassermann EM, Priori A, Lang N, Antal A, Paulus W, Hummel F, Boggio PS, Fregni F, Pascual-Leone A (2008) Transcranial direct current stimulation: state of the art 2008. Brain Stimulation 1:206–223.
Nitsche MA, Paulus W (2001) Sustained excitability elevations induced by transcranial DC motor cortex stimulation in humans. Neurology 57:1899–1901.
Onton J, Delorme A, Makeig S (2005) Frontal midline EEG dynamics during working memory. Neuroimage 27:341–356.
Pascual-Marqui RD (2002) Standardized low-resolution brain electromagnetic tomography (sLORETA): technical details. Methods Find Exp Clin Pharmacol 24:5–12.
Pashler H (1988) Familiarity and visual change detection. Perception Psychophys 44:369–378.
Rouder JN, Morey RD, Morey CC, Cowan N (2011) How to measure working memory capacity in the change detection paradigm. Psychon Bull Rev 18:324–330.
Roux F, Uhlhaas PJ (2014) Working memory and neural oscillations: alpha–gamma versus theta–gamma codes for distinct WM information? Trends Cognit Sci 18:16–25.
Sauseng P, Klimesch W, Heise KF, Gruber WR, Holz E, Karim AA, Glennon M, Gerloff C, Birbaumer N, Hummel FC (2009) Brain oscillatory substrates of visual short-term memory capacity. Curr Biol 19:1846–1852.
Sauseng P, Peylo C, Biel AL, Friedrich EVC, Romberg-Taylor C (2019) Does cross-frequency phase coupling of oscillatory brain activity contribute to a better understanding of visual working memory? Br J Psychol 110:245–255.
Siebenhühner F, Wang SH, Palva JM, Palva S (2016) Cross-frequency synchronization connects networks of fast and slow oscillations during visual working memory maintenance. Elife 5 e13451.
Siegel M, Warden MR, Miller EK (2009) Phase-dependent neuronal coding of objects in short-term memory. Proc Natl Acad Sci 106:21341–21346.
Todd JJ, Marois R (2005) Posterior parietal cortex activity predicts individual differences in visual short-term memory capacity. Cognit Affect Behav Neurosci 5:144–155.
Tort AB, Komorowski R, Eichenbaum H, Kopell N (2010) Measuring phase-amplitude coupling between neuronal oscillations of different frequencies. J Neurophysiol 104:1195–1210.
Tsai FF, Fan SZ, Lin YS, Huang NE, Yeh JR (2016) Investigating power density and the degree of nonlinearity in intrinsic components of anesthesia EEG by the Hilbert-Huang transform: an example using ketamine and alfentanil. PLoS ONE 11.
Tseng P, Chang Y-T, Chang C-F, Liang W-K, Juan C-H (2016) The critical role of phase difference in gamma oscillation within the temporoparietal network for binding visual working memory. Sci Rep 6:1–15.
Tseng P, Hsu TY, Chang CF, Tzeng OJL, Hung DL, Muggleton NG, Walsh V, Liang WK, Cheng SK, Juan CH (2012) Unleashing potential: transcranial direct current stimulation over the right posterior parietal cortex improves change detection in low-performing individuals. J Neurosci 32:10554–10561.
Tseng P, Wang M-C, Lo Y-H, Juan C-H (2018) Anodal and cathodal tDCS over the right frontal eye fields impacts spatial probability processing differently in pro-and anti-saccades. Front Neurosci 12:421.
Turi Z, Alekseichuk I, Paulus W (2018) On ways to overcome the magical capacity limit of working memory. PLoS Biol 16.
Unsworth N, Engle RW (2007) The nature of individual differences in working memory capacity: active maintenance in primary memory and controlled search from secondary memory. Psychol Rev 114:104–132.
Unsworth N, Engle RW (2008) Speed and accuracy of accessing information in working memory: an individual differences investigation of focus switching. J Exp Psychol-Learn Memory Cognit 34:616–630.
van Ede F, Niklaus M, Nobre AC (2017) Temporal expectations guide dynamic prioritization in visual working memory through attenuated alpha oscillations. J Neurosci 37:437–445.
Vidaurre D, Hunt LT, Quinn AJ, Hunt BA, Brookes MJ, Nobre AC, Woolrich MW (2018) Spontaneous cortical activity transiently organises into frequency specific phase-coupling networks. Nat Commun 9:1–13.
Vogel EK, Machizawa MG (2004) Neural activity predicts individual differences in visual working memory capacity. Nature 428:748–751.
Vogel EK, McCollough AW, Machizawa MG (2005) Neural measures reveal individual differences in controlling access to working memory. Nature 438:500–503.
Vosskuhl J, Huster RJ, Herrmann CS (2015) Increase in short-term memory capacity induced by down-regulating individual theta frequency via transcranial alternating current stimulation. Front Hum Neurosci 9.
Witkowski M, Garcia-Cossio E, Chander BS, Braun C, Birbaumer N, Robinson SE, Soekadar SR (2016) Mapping entrained brain oscillations during transcranial alternating current stimulation (tACS). Neuroimage 140:89–98.
Wolinski N, Cooper NR, Sauseng P, Romei V (2018) The speed of parietal theta frequency drives visuospatial working memory capacity. PLoS Biol 16.
Woodman GF, Vecera SP, Luck SJ (2003) Perceptual organization influences visual working memory. Psychon Bull Rev 10:80–87.

APPENDIX A. SUPPLEMENTARY DATA

Supplementary data to this article can be found online at https://doi.org/10.1016/j.neuroscience.2021.02.013.

(Received 25 September 2020, Accepted 8 February 2021)
(Available online xxxx)